

NASA Technical Paper 1177

COMPLETED
ORIGINAL

Theoretical Contamination of Cryogenic Satellite Telescopes

M. Murakami

APRIL 1978

NASA

NASA Technical Paper 1177

Theoretical Contamination of Cryogenic Satellite Telescopes

M. Murakami
Ames Research Center
Moffett Field, California



National Aeronautics
and Space Administration

**Scientific and Technical
Information Office**

1978

THEORETICAL CONTAMINATION OF CRYOGENIC SATELLITE TELESCOPES

M. Murakami*

Ames Research Center

SUMMARY

Contamination has two undesirable effects on infrared telescope systems. First, absorption and scattering can be caused by deposition of condensible gas molecules on cooled surfaces; second, radiation emission and absorption can come from solid particles and molecules surrounding the satellite. This paper is concerned with the former effect on the optical elements of large IR telescope (about 1 m in diameter) cooled to about 20 K. The state of contaminant molecules, the deposition rate on key surfaces, and the heat-transfer rate are estimated by the use of a zeroth-order approximation. Optical surfaces of infrared telescopes cooled to about 20 K should be considered to be covered with at least several deposition layers of condensible molecules without any contamination controls. The effectiveness of the purge gas method of contamination control is discussed. This method attempts to drive condensible molecules from the telescope tube by impacts with a purging gas in the telescope tube. For this technique to be sufficiently effective, the pressure of the purged gas must be more than 2×10^{-6} torr. The influence caused by interactions of the purge gas with the particulate contaminants are found to slightly increase the resident times of the particulate contaminants within the telescope field of view. Numerical results are presented for the Shuttle Infrared Telescope Facility (SIRTF) orbiting at an altitude of 350,400 km.

1. INTRODUCTION

If a high-sensitivity infrared telescope is to be used in manned space flight, the effects of contamination on such an instrument must be understood. Three kinds of contaminants can interfere with the operation of an IR telescope in space: the first is caused by the deposition of condensible gas molecules on cooled surfaces; the second, by radiation emission from solid particles crossing the field of view; the third, by radiation emission, absorption, and scattering from gaseous molecules within the field of view. The first type of contamination may degrade the performance of the telescope because of radiation reflecting and scattering off the layer deposited on the optical surfaces. This type of contamination is the subject of this report. Contamination criteria have been recommended by the NASA Astronomy Working Group (refs. 1 and 2), and there have been several numerical evaluations

*National Research Council Research Associate; presently at the Institute of Space and Aeronautical Science, University of Tokyo, Tokyo, Japan.

(ref. 3) of the Shuttle contamination. Here the Shuttle Infrared Telescope Facility (SIRTF) was used as an example, although the results are generally applicable. The objectives of this investigation were to estimate the physical state of the condensible contaminant around the Shuttle, to present a basic description of the adsorption and condensation phenomena on cooled surfaces in space, and to evaluate the effectiveness of the purge gas method of contamination control.

2. PHYSICAL STATE OF GASEOUS CONTAMINANT

2.1 Origin of Contaminants

Condensible molecules may be classified into two groups: either ambient molecules or molecules that originate from the satellite. The latter group includes molecules from thrusters and vent systems as well as those that are outgassed from surfaces of the satellite. Some of these molecules may be incident on a satellite without gaseous collisions before incidence. Molecules from thrusters and vent systems have strong direction-dependent properties with respect to the satellite motion. Molecules arriving directly from thrusters and vent systems may be basically excluded from consideration since the telescope systems are positioned on the vehicle to prevent such direct contamination. The contaminants from the satellite which are considered are the molecules that return to the satellite because of collisions with ambient molecules and those that are reflected from the satellite's surfaces. Molecules may be treated individually according to their origins because there is little mutual interaction. The ambient molecules are characterized by their high kinetic energy, high flux rate, and the common velocity with respect to the satellite (see table 1.) They could cause a contamination problem, but their influence can be minimized if the axis of the telescope is not pointed in the direction of the satellite velocity vector. The term "return molecules" is used here to designate molecules that originate from the satellite and return to it because of collisions and reflections.

2.2 Physical State of Contaminant

2.2.1 *Return flux rate*— Knowledge of the return flux rate is needed to estimate the surface deposition rate. This complex quantity is a function of time, altitude, satellite attitude, the activity of the satellite exhaust systems, and thruster activity. Several numerical results of the return molecule mass flux rate (\dot{m} , g/cm²-sec) are given in table 2 (ref. 3). Here the coordinate system is defined as in figure 1 and VERN and EVP represent the 11.3-kg (25-lb) thrust vernier engines and the water evaporator, respectively. The worst case shows a strong angular dependent property chiefly caused by the molecules that reflect from the wings. The background is almost uniformly distributed in space except the sharp peak resulting from the return molecules caused by collisions with the ambient molecules. The number flux rate N is related to the mass flux rate \dot{m} as follows:

$$N = \dot{m} \frac{N_{AV}}{M} \quad (1)$$

where N , N_{AV} , and M are the number flux rate ($1/\text{cm}^2\text{-sec}$), Avogadro number, and molar weight, respectively. Figure 2 shows the relation between \dot{m} and N .

2.2.2 Physical state of return flux— Besides the flux rate, the temperature of the return molecules must be known to investigate the contamination. As an approximation, the temperature of reflected molecules from the Shuttle surfaces is considered to be the same as the temperature of the Shuttle surfaces because the energy accommodation coefficient α_e of the surface is the order of 1 when it is contaminated by adsorbed molecules as in the present case (ref. 4). The number density and pressure at the telescope are given by

$$n_{cr} = 2\sqrt{\pi h_{cr}} N_{cr} = \frac{2\sqrt{\pi} N_{cr}}{C_{mcr}} \quad (2)$$

$$P_{cr} = n_{cr} k T_{cr} \quad (3)$$

$$h = \frac{m}{2kT}$$

where C_m (most probable speed) is given by $1/\sqrt{h}$.

Molecules emanating from the shuttle will likely collide only once with one of the ambient molecules before returning to the shuttle. The hard-sphere collision is considered for simplicity, though this is an *a priori* assumption. A collision between hard spheres is illustrated in figure 3, where \bar{V}_a and \bar{V}_c are the velocities of an ambient molecule and of a contaminant, respectively. Collision dynamics for this model show that the velocity \bar{V}_c' after a collision is given with the aid of the velocity of the center of mass, $\bar{V}_{c/m}$, as

$$\bar{V}_c = \bar{V}_{c/m} + \frac{m_a}{m_c + m_a} g\bar{n} \quad (4)$$

$$\bar{V}_{c/m} = \frac{m_c \bar{V}_c + m_a \bar{V}_a}{m_c + m_a}$$

where g and \bar{n} are given by

$$g = |\bar{g}| = |\bar{V}_c - \bar{V}_a| \quad (5)$$

$$g\bar{n} = \bar{V}_c' - \bar{V}_a' \quad (6)$$

The unit vector \bar{n} is uniformly distributed. We may regard $\bar{V}_a = 0$ and $\bar{V}_c = \bar{V}_s$. Thus the velocities of return molecule with respect to the Shuttle system become

$$\bar{U}_c = \frac{m_a \bar{V}_c}{m_c + m_a} - \frac{m_a}{m_c + m_a} V_c \bar{n} \quad (7)$$

This model calculation shows that the return molecules have a large mean velocity $m_a \bar{V}_c / (m_c + m_a)$, and that the thermal velocity is roughly approximated by $m_a V_c / (m_c + m_a)$.

2.2.3 Flux rate on telescope surfaces—An estimate of the deposition rate for a uniform distribution of the flux with zero mean velocity is first presented as an example. This idealized estimate shows the effect of the configuration of the telescope tube on the flux rate, although the distribution is actually highly asymmetrical because of the large mean velocity (as mentioned in the previous section). A view factor, identical to that used in radiation heat transfer, can be used because the return molecules are in free molecular flow. The incident flux on surface 2, N_2 , as shown in figure 4, is computed in terms of a view factor F_{2-1} (see appendix A):

$$N_2 = N_1 F_{2-1} \quad (8)$$

The flux on the tube wall (surface 3) at a distance x from the aperture is written similarly as

$$N_3^w = N_1 F_{\delta 3-1} \quad (9)$$

The results are shown in figure 5 as a function of $L/2a_3$ or $x/2a_3$, respectively, where $a_3 = 59.3$ cm and $a_4 = 29.3$ cm. Figure 5 shows that the incident flux rate on the first mirror is 3.7% of the original incident flux rate, N_1 , and the flux rate on the tube wall varies from 50% of N_1 at the aperture to 0.3% at the bottom of the tube. Likewise, the flux rate on the inner tube wall (surface 4) is given by

$$\begin{aligned} N_4^w &= N_1 F_{\delta 4-1} \\ &= -N_1 \left(\frac{a_3^2 - a_4^2}{2a_4} \frac{dF_{2-1}}{dx} + \frac{a_3}{a_4} F_{\delta 3-1} \right) \end{aligned} \quad (10)$$

The effect of a sunshade would only slightly decrease these values. However, when the telescope points in the direction of satellite motion, the sunshade would act much like a funnel and would greatly increase the mass flux into the telescope. Note that reflections of the contaminant on cold solid surfaces are not likely to occur because of the large value of the sticking coefficient of the surfaces.

The contribution of the mean velocity of the contaminant to the flux rate becomes prominent as the inclination angle ψ increases (fig. 6). This was examined for the simple case of a cylinder with a diameter $2a_3 = 159.6$ cm and a length of $L = 508$ cm. The oncoming flux is assumed to have a Maxwellian distribution with the mean velocity \bar{U}_1 :

$$f_i = n_i \left(\frac{h_i}{\pi} \right)^{3/2} \exp[-h_i (\bar{v} - \bar{u}_i)^2] \quad (11)$$

$$h_i = \frac{m_i}{2kT_i}$$

where subscript i indicates the collided molecules (c) including both contaminant and ambient molecules or the ambient molecules (a) incident without collisions. The parameters h_c and \bar{u}_c are approximately given from the results of section 2.2.2.

The incident flux to a point (x_2, y_2) on the bottom coming directly from the aperture without experiencing reflection on surfaces is computed by

$$N_2(x_2, y_2) = - \int (\bar{v} \cdot \bar{n}_2) f_i d\bar{v} \quad (12)$$

$$= L^2 n_i \left(\frac{h_i}{\pi} \right)^{3/2} e^{-h_i U_i^2} \int_0^{2\pi} \int_0^{a_3} \left[\frac{A}{2h_i} + \frac{1}{2h_i^2} \right. \\ \left. + e^{h_i A^2} \left(\frac{3A}{2h_i} + A^3 \right) \int_{-A}^{\infty} e^{-h_i t^2} dt \right] \frac{r_i}{r_{12}^4} d\eta_1 dr_1 ; \quad \bar{v} \cdot \bar{n}_2 < 0 \quad (13)$$

$$A = -U_i (\sin \phi \cos \theta \cos \psi - \cos \phi \sin \psi)$$

$$\sin \phi = \frac{r_3}{r_{12}}$$

$$\cos \phi = \frac{L}{r_{12}}$$

$$\cos \theta = \frac{r_1 \cos \eta_1 - x_2}{r_3}$$

$$r_3 = \sqrt{(x_2 - r_1 \cos \eta_1)^2 + (y_2 - r_1 \sin \eta_1)^2}$$

$$r_{12} = \sqrt{r_3^2 + L^2}$$

where a point on the aperture is specified by r_1 and η_1 as shown in figure 6. The results are shown in figures 7(a) and (b). The flux rate is made dimensionless with respect to a flux rate, $n_i/(2\sqrt{\pi}h_i)$, at the aperture when $U_i = 0$. In figure 7(a), dimensionless flux rates are plotted against

the telescope inclination angle (ψ) for collided molecules and ambient molecules. The contribution of the direct incidence of ambient molecules is smaller than that of collided molecules when $\psi < 60^\circ$, although $n_1/(2\sqrt{\pi}h_1)$ for ambient molecules is almost one order larger than that for collided molecules. Figure 7(b) shows the flux-rate distribution along the x_2 -axis on the primary mirror. The distribution is not uniform for ambient molecules. The flux rate including contaminant and ambient molecules increases by more than an order of magnitude when ψ changes from 0° to 60° . The effect of the mean velocity thus makes it difficult for molecules to reach the bottom for smaller values of ψ , but it strongly increases the incident flux rate at the bottom for $\psi > 60^\circ$. Besides the molecules coming directly from the aperture without collisions, those reflected on the telescope tube or baffle are incident on a key surface. The quantitative feature of the contribution of such molecules is similar to that of directly incident molecules.

2.3 Constituents of Condensible Contaminant

Possible constituents and quantities of gaseous contaminants have been estimated (ref. 3). The contaminants are mainly H_2O , O_2 , CO , CO_2 , H_2 , NO , OH^- , O^+ , and hydrocarbons. The contamination treated here concerns adsorption and condensation on key low-temperature surfaces. Chemical adsorption or reaction may occur on surfaces when molecules and particles strike the surfaces at very high speeds. The effects of H_2O and CO_2 molecules among the possible constituents studied in connection with the performance of optics (refs. 5-12) have been found to cause serious problems. The effects of the other constituents have not been investigated.

3. ADSORPTION/CONDENSATION

3.1 Adsorption/Condensation of Contaminants

The adsorption-desorption phenomenon is physically different from condensation/sublimation, but we treat the two phenomena similarly from the qualitative point of view since our concern lies mainly in the deposition rate and the heat exchanged, not the mechanism. The significant difference is that the desorption energy is larger than the sublimation energy. The molecules deposited on a surface, regardless of their state, influence the gas-surface interaction as well as the optical properties of the surface. The interaction, in turn, influences the deposition rate, and so on. However, the present case can be greatly simplified.

First, the cooled surface of the telescope may be regarded as being covered with at least a molecular monolayer. (This assumption is justified later.) Because of this deposition, the interaction potential is smaller than the desorption energy of a pure gas-solid interaction. The desorption energy is approximately one order of magnitude larger than the sublimation energy at the same temperature. Thus, the condensation energy may be used regardless of whether it is adsorption or condensation. Second, almost all

the molecules (except helium) incident on the cooled surface are captured because the sticking coefficient is close to unity. Third, the deposited molecules will form an amorphous structure on a solid surface. The surface diffusion of captured molecules is very limited because of the low temperatures.

The deposition rate is found as a function of the incident flux rate (N). The adsorption rate (N_a) is expressed in terms of the sticking coefficient α_s and the surface coverage θ_s by

$$N_a = \alpha_s (1 - \theta_s) N \quad (14)$$

The desorption rate (N_d) is given by

$$N_d = \rho_a \theta_s \nu_o e^{-q/kT} \quad (15)$$

where ρ_a , ν_o , and q are surface density (molecules/cm²), desorption frequency ($\approx 10^{12} - 10^{13}$ /sec), and desorption energy, respectively. Therefore, the net adsorption rate (N_{net}) results in

$$N_{net} = \alpha_s (1 - \theta_s) N - \rho_a \theta_s \nu_o e^{-q/kT} \quad (16)$$

The incident flux (N) is given by

$$N = \frac{P}{(2\pi mkT)^{1/2}} \quad (17)$$

If the system is at equilibrium, then $N_{net} = 0$, and the value of θ_s is

$$\theta_s = \frac{bP}{1 + bP} ; \quad b = \frac{\alpha_s e^{-q/kT}}{\rho_a \nu_o (2\pi mkT)^{1/2}} \quad (18)$$

which is the Langmuir formula for monolayer adsorption. The BET equation, which is a mathematical model to predict the surface coverage, for the multilayer adsorption is derived basically by applying the above idea to each layer. However, the BET equation is inconsistent when two or more components are present. According to the BET equation, the desorption rate will increase when the surface is contaminated with molecules because of a decrease in desorption energy. Recent investigations (refs. 13 and 14) have found this to be only partially correct.

This inconsistency seems to be solved by considering the structure of the deposition layer as well as the variation of desorption or sublimation energy. In the derivation of the BET equation, the site where a molecule should be adsorbed must be the top dead center of a preadsorbed molecule or on the bare surface, as shown by figure 8(a). Thus, the total site number

over the layer must be equal to ρ_a . If this restriction is relaxed, the number of sites will increase. Likewise, the number of adsorbed molecules will also increase in comparison with that predicted by the BET equation under the same conditions. This situation seems to be realized in the present case. It may be realized by considering the amorphous structure of the deposited molecules caused by the lack of surface (or two-dimensional) diffusion and by the different molecular sizes. Such a deposition is envisioned in figure 8(b).

When the vapor pressure above the phase surface exceeds the saturation vapor pressure corresponding to the surface temperature, the sublimation/condensation theory will predict the deposition rate. The condensation rate is expressed in a form similar to equation (14), except $\theta_s = 0$ because an incident molecule can condense anywhere over the phase surface. This may be considered an extreme case of maximum adsorption because the number of sites is not restricted by previously deposited molecules. Thus, the deposition rate is

$$N_c = \alpha_s N \quad (19)$$

The sublimation rate is computed using kinetic theory if it is assumed that the distribution of the sublimating molecules is Maxwellian with a zero mean velocity corresponding to the saturation vapor pressure at the surface temperature. The sublimation rate is then

$$N_s = \frac{\alpha_s P}{(2\pi mkT)^{1/2}} \quad (20)$$

and the net deposition rate becomes

$$N_{net} = \alpha_s N - \frac{\alpha_s P}{(2\pi mkT)^{1/2}} \quad (21)$$

The energy exchange relating to adsorption or condensation can be evaluated. Deposition of an ideal gas molecule with zero mean velocity on a cooled surface releases energy according to

$$e_d = q - e_s + \Delta e_k$$

where e_d is the energy released on adsorption or condensation, q is the potential energy released, e_s is the energy possessed by a deposited molecule, and Δe_k is the sum of both energy differences of translation Δe_m and rotation Δe_{rot} during deposition. The term e_d is also called the "differential heat of deposition." The quantity e_s is negligibly small in this case. The amount of Δe_{tr} is $1/2 kT$ for ideal monolayer adsorption when only one degree of freedom of translation perpendicular to the surface is lost; Δe_{tr} is $3/2 kT$ for condensation. The quantity Δe_{rot} is expressed in terms of the number of rotational degrees of freedom i_{rot} as

$$\Delta e_{\text{rot}} = \frac{1}{2} kT \ell_{\text{rot}}$$

The classical equipartition law of energy is used. The energy flux rate due to deposition or condensation is computed from e_d multiplied by the incident flux rate N_a or N_c for either adsorption or condensation. The net energy flux rate E is determined as the sum of the energy fluxes due to deposition and energy accommodation. The latter E_{ac} is computed in terms of the accommodation coefficient α_e from kinetic theory, assuming that $\alpha_T = 1.0$, as

$$E_{ac} = 2k\alpha_e (1 - \alpha_s) N T_c (1 - T_d/T_c) \quad (22)$$

where subscript d corresponds to the surface of the deposition layer. For adsorption-desorption,

$$\begin{aligned} E &= \left[q + \frac{1}{2} kT_c (1 + \ell_{\text{rot}}) \right] N_a \\ &\quad - \left[q + \frac{1}{2} kT_d (1 + \ell_{\text{rot}}) \right] N_d + E_{ac} \\ &= qN_{\text{net}} + \frac{1}{2} k(1 + \ell_{\text{rot}}) (T_c N_c - T_d N_d) + E_{ac} \end{aligned} \quad (23)$$

For condensation/sublimation,

$$\begin{aligned} E &= \left[q + \frac{1}{2} kT_c (3 + \ell_{\text{rot}}) \right] N_c \\ &\quad - \left[q + \frac{1}{2} kT_d (3 + \ell_{\text{rot}}) \right] N_s + E_{ac} \\ &= qN_{\text{net}} + \frac{1}{2} k(3 + \ell_{\text{rot}}) (T_c N_c - T_d N_d) + E_{ac} \end{aligned} \quad (24)$$

In both cases, the first term is expressed hereafter as E_d and the second, as E_k . Note that T_c is sufficiently larger than T_d and even $N_c \gg N_s$ for several constituents. (The numerical evaluation of these values is given in section 3.3.)

3.2 Effects of Cryodeposit on Surface Optical Properties

A cryodeposit on a solid surface may change its emissivity, reflectance, and transmittance (refs. 5-12). As a result, radiation absorption and scattering may occur on the telescope mirror and thereby raise its temperature. One of the requirements determined by the Astronomy Working Group is that the radiation loss due to absorption by condensibles on optical surfaces for $\Delta\lambda/\lambda = 0.1$ bandwidth in the optical and IR be less than 1% for the entire mission. This general criterion seems to correspond to the more

explicit criterion that the tolerable thickness of water deposition (ice) is less than $0.2 \mu\text{m}$ at 77 K, according to experimental data (ref. 5). Also, in the thickness range $0-2.5 \mu\text{m}$, the emissivity increase per unit film thickness is highest for water, followed in order by aliphatic hydrocarbons, silicone oil, aromatic hydrocarbons, and carbon dioxide.

It is uncertain that these conclusions deduced from an experiment at 77 K are applicable at 20 K. But the numerical evaluations that follow are based on the 77 K data. The time required for deposition up to a critical thickness is easily given in terms of the time for the monolayer formation. The number flux rate N_1 is approximately $10^{12}-10^{15}$ molecules/ $\text{cm}^2\text{-sec}$ (fig. 2) if all return molecules are H_2O . The monolayer coverage ρ of H_2O molecules is about $8 \times 10^{14}/\text{cm}^2$ since its diameter (d) is about 2.9 \AA (ref. 15).

$$\rho = \frac{1}{\pi d^2/2} = 8 \times 10^{14}/\text{cm}^2$$

Then, the time required for monolayer formation can be computed as

$$t_0 = \frac{\rho}{N_1 F} \quad (25)$$

Here, F is the view factor given in section 2.2.3. All molecules incident on surfaces are assumed to be captured. The results are given in table 3 with N_1 and F as parameters. A simple estimate gives the time for the deposition to pile up to $0.2 \mu\text{m}$:

$$t(0.2 \mu\text{m}) = \frac{0.2 \times 10^{-4}}{\sqrt{1/\rho}} t_0 = 6 \times 10^2 t_0$$

The time t_0 (given in table 3) is very small compared with telescope operation period. Because of this, the cooled surfaces of all space IR telescopes may be considered to be always covered with at least one monolayer of condensed molecules, which justifies an earlier assumption. If the backscattered H_2O flux is $10^{12}/\text{cm}^2/\text{sec}$, then the time to deposit $0.2 \mu\text{m}$ near a forward baffle ($F = 1$) is 130 hr, while the time to coat a portion of the primary mirror of a telescope ($F = 0.05$) is 2,500 hr. Thus problems arise with the baffle if the mission exceeds 7 days or if the backscattered flux exceeds $10^{12}/\text{cm}^2/\text{sec}$.

3.3 Evaluation of Heat-Transfer Rates for Deposition of CO_2 , CO , N_2 , O_2 , H_2O , and H_2

The heat-transfer rate is estimated for several candidate components. Values of the sticking coefficient α_s , the thermal accommodation coefficient α_e , and the tangential momentum accommodation coefficient α_t are taken to be unity for every gas except He and H_2 , because the data are incomplete and inconclusive. Except for He, the temperature of the deposition layer, T_d ,

is taken to be 20 K. The vapor pressure and the sublimation energy are given in tables 4 and 5, respectively. The heat of adsorption is approximated to be several times the heat of sublimation. The sticking coefficient data used are shown in tables 6-8. Note that the sticking coefficient data for deposition on pure (not contaminated) solid surfaces are omitted because such values are considerably smaller than those for contaminated surfaces. The heat-transfer rates to the wall are shown in tables 9 and 10, with the flux rate N of each constituent as a parameter. (Several key data employed for this purpose are shown below.)

Carbon Dioxide

$$\alpha_e = \alpha_r = 1.0$$

$$l_{\text{rot}} = 2$$

$$T_c \text{ is assumed to be } 600 \text{ K}$$

Heat of sublimation, -6.5 kcal/gmole

Carbon Monoxide

$$\alpha_e = \alpha_r = 1.0$$

$$l_{\text{rot}} = 2$$

$$T_{\text{CO}} = 600 \text{ K}$$

Nitrogen

$$\alpha_e = \alpha_r = 1.0$$

$$l_{\text{rot}} = 2$$

$$T_{\text{CO}_2} = 600 \text{ K}$$

Oxygen

$$\alpha_e = \alpha_r = 1.0$$

$$l_{\text{rot}} = 2$$

$$T_{\text{O}_2} = 600 \text{ K}$$

Water

$$\alpha_e = \alpha_r = 1.0$$

$$l_{\text{rot}} = 3$$

$$T_{\text{H}_2\text{O}} = 600 \text{ K}$$

Heat of sublimation is assumed to be 12 kcal/gmole.

3.3.1 *Heat-transfer result*— It may be concluded from these estimates that the heat input rate to the surface from the contamination process will not exceed 5×10^{-7} cal/cm²/sec. This value is compared to a blackbody emissive power at 20 K of 2.2×10^{-7} cal/cm²/sec.

4. PURGED-GAS FLOW

4.1 Requirement for Gas Flow

The idea of controlling contamination by purging gas from the telescope barrel opposing to the contaminant flux is based on the momentum change of

contaminant molecules due to collisions with the purged-gas molecules. The change in momentum is examined when a gas molecule belonging to group C (contaminant) collides with a molecule from group G (gas). A physical model is illustrated in figure 9, where the gas G flows from left to right. The X axis is taken along the mass velocity U_c . The momentum flux rate (momentum/cm²-sec) of the contaminant flux (c) at X is $m_c U_c N_c$, where $N_c = n_c U_c$. The variation of the velocity of a molecule from group C per collision is

$$\frac{m_G}{m_c + m_G} (1 - \cos \chi) \bar{g}_{cG}$$

where χ and \bar{g}_{cG} are the deflection angle of collision and the relative velocity of the two molecules, respectively. The average change in momentum flux of the gas C after N_c collisions is

$$N_c \frac{m_c m_G}{m_c + m_G} \bar{g}_{cG} \int (1 - \cos \chi) b db d\epsilon = N_c \frac{m_c m_G}{m_c + m_G} \bar{g}_{cG} \sigma^{(1)}(\bar{g}_{cG}) \quad (26)$$

where b and ϵ are the collision parameters, $\bar{g}_{cG} = |\bar{g}_{cG}|$, and $\sigma^{(1)}$ is the collision cross section. Thus, the total momentum change of the gas C within a slab with thickness δx is approximately given by

$$N_c \frac{m_c m_G}{m_c + m_G} \bar{g}_{cG} \sigma^{(1)} n_G \left(1 + \frac{U_G}{U_c}\right) \delta x = N_c \frac{m_c m_G}{m_c + m_G} \frac{U_c + U_G}{\lambda_{cG}} \delta x \quad (27)$$

The quantity λ_{cG} is the mean free path of gas C with respect to gas G and is equal to $U_c / (\sigma^{(1)} n_G \bar{g}_{cG})$. This equation is used to evaluate the momentum change of the contaminant caused by collisions with the purge gas in section 4.3.1. Equation (27) provides the conclusion that a heavy gas with a high mean velocity is desirable for a purging gas. Unfortunately, heavy gases condense at the required optics temperature and hot gases would warm the optics. The flow characteristics of both the contaminant and the purge gas and the required quantity of the purge gas are roughly found if one examines the Knudsen numbers of the flows. In terms of the tube diameter $2a_3$, the Knudsen number can be written:

$$K_{nG} = \frac{\lambda_{GG}}{2a_3} \quad (28)$$

where λ_{GG} is the mean free path, which is defined in terms of the heat conductivity k as

$$\lambda_{GG} = \frac{4}{5\sqrt{\pi}} \frac{m_G}{k P_G} \sqrt{\frac{1}{h_G}} k \quad (29)$$

Also the heat conductivity k is uniquely related to the viscosity η according to $k = 15k\eta/4m$. An estimate of Knudsen number and flow regime as a function of pressure is shown in figure 10 for helium at 20 K. Figure 10 also shows K_{nc} , which is discussed later. The values of k and $2a_3$ are taken to be 2.6×10^3 ergs/sec-cm-K and 119 cm, respectively. The mean free path λ_{CG} of the contaminant with respect to the purge gas is defined by

$$\lambda_{CG} = \frac{U_c}{\sigma_{CG} n_G g_{CG}} \quad (30)$$

and the collision cross section σ_{CG} is approximated by

$$\sigma_{CG} = \sigma_{GC} = \frac{\pi}{4} \left(\sqrt{\frac{\sigma_c}{\pi}} + \sqrt{\frac{\sigma_{GG}}{\pi}} \right)^2 \quad (31)$$

Since no data on σ_{CG} are available, σ_c and σ_{GG} are approximately given by $\sqrt{2}\pi d_c^2$ and $\sqrt{2}\pi d_G^2$, where d_c and d_G are the respective molecular diameters. The parameters necessary to compute λ_{CG} are

$$\begin{aligned} d_c &= 3.7 \text{ \AA} & m_c &= 4.8 \times 10^{-23} \text{ g} & \left. \begin{array}{l} d_c = 3.7 \text{ \AA} \\ m_c = 4.8 \times 10^{-23} \text{ g} \end{array} \right\} & \text{Air} \\ d_G &= 2.7 \text{ \AA} & & & & \text{K (helium)} \\ \sigma_{CG} &= 4.5 \times 10^{-15} \text{ cm}^2 \\ T_c &= 600 \text{ K} \\ U_c &= \frac{1}{2\sqrt{\pi h_c}} = 1.7 \times 10^4 \text{ cm/sec} \\ T_G &= 20 \text{ K} \\ g_{CG} &= U_c + U_G = U_c + \sqrt{\frac{\gamma k T_G}{m_G}} = 4.3 \times 10^4 \text{ cm/sec} \\ & & (\gamma = \frac{5}{3}), U_G: & \text{speed of sound (assumed)} \\ n_G &= \frac{P_G}{k T_G} = 4.8 \times 10^{17} \times P_G \text{ (torr)} \quad 1/\text{cm}^3 \end{aligned}$$

Thus,

$$\lambda_{CG} = \frac{1.8 \times 10^{-4}}{P_G \text{ (torr)}} \quad (\text{cm}) \quad (32)$$

The mean number of collisions experienced by a contaminant molecule as it travels over an interval L , which is the telescope length, is given by the reciprocal of a different Knudsen number defined by

$$K_{nc} = \frac{\lambda_{CG}}{L} = \frac{7.1 \times 10^{-7}}{P_G (\text{torr})} \quad (33)$$

This Knudsen number is also shown in figure 10. The magnitude of $1/K_{nc}$ must exceed unity for a purged-gas system to be effective. The working gas is assumed to be helium at $T_G = 20$ K, flowing at the speed of sound. The total mass-flux rate is given as a function of pressure and Mach number M_G as

$$\begin{aligned} \dot{m}_G &= m_G n_G M_G \sqrt{\frac{\gamma k T_G}{m_G}} = P_G M_G \sqrt{\frac{\gamma m_G}{k T_G}} \\ &= 8.3 \times 10^{-2} M_G P_G (\text{torr}) \quad \text{g/cm}^2\text{-sec} \end{aligned}$$

where the quantities in this equation are those at the telescope aperture. The gas velocity is expressed by the speed of sound multiplied by the Mach number M_G . The total mass-flow rate required for a purged-gas pressure of $P_G = 3 \times 10^{-6}$ torr 7.5 g/hr for a telescope with a 119-cm aperture at $M_G = 1.0$.

4.2 Tube Flow at Low Pressure

Rarefied gas flow inside a tube is now examined. The Knudsen number in the tube must be less than 1 if the purged-gas flow is to be effective in contamination control. Flow that is effused from a large reservoir with very small mean velocity and then is accelerated by the pressure difference in the tube will have a nearly flat velocity profile because of the large slip at the wall (refs. 29-34). This type of flow is usually choked at the aperture and thus its velocity is limited. Flow exhausted from diverging nozzles at the bottom of the telescope tube has been suggested to obtain high velocities.

The heat-flux rate to the tube wall from the purged gas can be computed with the aid of several assumptions. The distribution function of the gas is assumed to be Maxwellian and is therefore given by

$$f = n_G \left(\frac{h_G}{\pi} \right)^{3/2} \exp[-h_G (\bar{V} - \bar{U}_G)^2] \quad (34)$$

The second assumption, concerning the gas-surface interaction on the tube wall, is that $\alpha_T = 1.0$. The net heat-transfer rate is given as the difference between the incident energy E_i and that carried away by the reflected molecules E_r . It follows from the definition of the energy accommodation that

$$E_i - E_r = \alpha_e (E_i - E_w) \quad (35)$$

where subscript w shows quantities on surfaces. Mass conservation and the fact that $\alpha_r = 1.0$ yield the following relation for the number flux rate on the surface:

$$N_i = N_r = N_w = \frac{n_i}{2\sqrt{\pi}h_i} = \frac{n_G}{2\sqrt{\pi}h_G} \quad (36)$$

Then the net heat-flux rate becomes

$$\begin{aligned} E_i - E_r &= \frac{\alpha_e m_G}{2\sqrt{\pi}} \frac{n_G}{\sqrt{h_G}} \left(\frac{1}{h_G} - \frac{1}{h_w} \right) \\ &= \frac{\alpha_e P_G}{\sqrt{\pi}h_G} \left(1 - \frac{T_w}{T_G} \right) \end{aligned} \quad (37)$$

In figure 11, the numerical result is presented as a function of $\alpha_e P_G$ and T_G for $T_w = 20$ K.

4.3 Interaction of Contaminant with Purged Gas

As described previously, the effectiveness of the purged-gas system of contamination control depends both on the number of collisions of the contaminant molecules with purged-gas molecules and on the magnitude of the momentum exchange during collision. A measure of the number of collisions is defined by equation (33) and the momentum change by equation (27). The flow field of the purged gas consists of the nearly parallel flow in the annular tube, followed by expansion into space through the sunshade. The application of the purged-gas method to contamination control aims to decrease the deposition rate on the tube surfaces and mirror, but the interaction of the purged gas with particulate contaminants may prolong the resident time of particles in the telescope field of view (FOV). This additional residence time is discussed later.

4.3.1 Interaction in the tube—Two mechanisms that change the state of the contaminant are (1) collisions with purged-gas molecules, and (2) deposition on the cooled surface. The contaminant flux is split into two such fluxes, called "virgin flux" and "collided flux," identified in the following discussion by subscripts ∞ and 0, respectively. The velocity distribution of the collided flux is assumed to be Maxwellian and is expressed by

$$f_0(x) = n_0(x) \left[\frac{h_0(x)}{\pi} \right]^{3/2} \exp[-h_0(x)(\vec{V} - \vec{U}_0)^2] \quad (38)$$

For a volume element with thickness δx at x (fig. 12), the incoming flux is $(N_0 + N_\infty)A$, while the outflow flux from the volume element is $(N_0 + \delta N_0 + N_\infty + \delta N_\infty)A + 2\pi\delta x[a_3(N_{30}^W + N_{3\infty}^W) + a_4(N_{40}^W + N_{4\infty}^W)]$, where A is the effective cross-sectional area for the contaminant flow field, which is $\pi(a_3^2 - a_4^2)$. The flux rates of the collided molecules incident to the telescope tube and to the baffle are N_{30}^W and N_{40}^W , respectively, and $N_{3\infty}^W$ and $N_{4\infty}^W$ are those of the virgin molecules. Mass conservation of the contaminant in the volume element yields

$$\delta N_0 + \delta N_\infty + \frac{2\pi\delta x}{A} [a_3(N_{30}^W + N_{3\infty}^W) + a_4(N_{40}^W + N_{4\infty}^W)] = 0 \quad (39)$$

The virgin flux is attenuated by collisions with purged-gas molecules and condensation on cooled surfaces. The quantity $N_\infty(\delta x/\lambda_{\infty G})A$ interacts in the control volume by collisions becoming part of the N_0 population; $\lambda_{\infty G}$ is the mean free path of the contaminant with respect to purged-gas molecules and $U_1 = U_c$. Mass conservation for the virgin flux yields

$$\delta N_\infty + \frac{2\pi\delta x}{A} (a_3 N_{3\infty}^W + a_4 N_{4\infty}^W) + N_\infty \frac{\delta x}{\lambda_{\infty G}} = 0 \quad (40)$$

A plausible assumption is introduced to evaluate $N_\infty(x)$:

$$\frac{N_\infty}{N_1 F_{x-1}} = \frac{N_{3\infty}^W}{N_1 F_{\delta 3-1}} = \frac{N_{4\infty}^W}{N_1 F_{\delta 4-1}} \quad (41)$$

where F_{x-1} , $F_{\delta 3-1}$, and $F_{\delta 4-1}$ are view factors (presented in Sec. 2.2.3) and N_1 is the incoming contaminant flux.¹

¹In the case without the purged gas,

$$N_\infty = N_1 F_{x-1}$$

$$N_{3\infty}^W = N_1 F_{\delta 3-1}$$

$$N_{4\infty}^W = N_1 F_{\delta 4-1}$$

These fluxes are attenuated by the collisions with the purged-gas molecules as follows:

$$N_\infty = N_1 F_{x-1} \cdot \alpha$$

$$N_{3\infty}^W = N_1 F_{\delta 3-1} \cdot \alpha_3 \quad (0 < \alpha, \alpha_3, \alpha_4 < 1.0)$$

$$N_{4\infty}^W = N_1 F_{\delta 4-1} \cdot \alpha_4$$

Thus, this assumption is equivalent to

$$\alpha = \alpha_3 = \alpha_4$$

Substitution of equations (10) and (41) into equation (40) yields

$$N_{\infty}(x) = N_1 F_{x-1}(x) \exp\left(-\frac{x}{\lambda_{\infty G}}\right) \quad (42)$$

Equation (39) can also be simplified to

$$\frac{dN_o}{dx} + \frac{2\pi}{A} (a_3 N_{30}^w + a_4 N_{40}^w) - N_{\infty} \frac{1}{\lambda_{\infty G}} = 0 \quad (43)$$

The flux rate N_{30}^w and N_{40}^w to the telescope tube are approximated by

$$N_{30}^w = N_{40}^w = \frac{m_G}{m_c + m_G} \frac{N_o(x)}{U_o(x)} [U_o(x) + U_G] \quad (44)$$

where $U_o(x)$ is the mean velocity of the collided molecule flux. Thus, equation (43) becomes

$$\frac{dN_o}{dx} + N_o \left(1 + \frac{U_G}{U_o(x)}\right) \frac{2(a_3 + a_4)}{a_3^2 - a_4^2} \frac{m_G}{m_c + m_G} - \frac{N_{\infty}}{\lambda_{\infty G}} = 0 \quad (45)$$

The decrease of momentum flux due to the collisions may be expressed in the form

$$- \left(N_o \frac{U_o + U_G}{\lambda_{oG}} + N_{\infty} \frac{U_1 + U_G}{\lambda_{\infty G}} \right) \frac{m_G}{m_c + m_G} \delta x$$

where

$$\lambda_{oG} = \frac{U_o(x)}{\sigma_{CG} n_G [U_o(x) + U_G]}$$

With equations (42) and (45), the equation of momentum flux is

$$\frac{N_{\infty}(x)}{\lambda_{\infty G}} \left(U_o - \frac{m_c U_1 - m_G U_G}{m_c + m_G} \right) + N_o \frac{dU_o}{dx} = - \frac{m_G}{m_c + m_G} N_o \frac{U_o + U_G}{\lambda_{oG}(x)} \quad (46)$$

Three equations, (42), (45), and (46), form a closed equation system that can be solved numerically for $N_{\infty}(x)$, $N_o(x)$, and $U_o(x)$. The boundary conditions are

$$\left. \begin{aligned} N_o(x) &= 0 \\ U_o(x) &= (m_c U_1 - m_G U_G) / (m_c + m_G) \\ N_{\infty}(x) &= N_1 \end{aligned} \right\} \quad \text{at } x = 0$$

These boundary conditions imply that all contaminant molecules that enter from the aperture condense on the telescope surfaces and the mirror when, in fact, some portion of the molecules is purged from the telescope tube by the purged gas. The total contaminant flux is

$$N(x) = N_{\infty}(x) + N_0(x) \quad (47)$$

and the total contaminant fluxes on the outer tube (surface 3) and the inner tube (surface 4) are, respectively, given by

$$N_3^W(x) = N_{30}^W(x) + N_{3\infty}^W(x) \quad (48)$$

$$N_4^W(x) = N_{40}^W(x) + N_{4\infty}^W(x) \quad (49)$$

Numerical results are shown in figure 13 where the total flux at the primary mirror (bottom), $N_2 = N(L)$, and the total flux on the telescope tube (bottom), $N_3^W(L)$, are given as a function of purged-gas pressure. The purged gas is assumed to be helium at 20 K, and the gaseous contaminant is assumed to be water vapor at 300 K. Computations shown in figure 13 are for two cases of the purged-gas flow velocity: first, the speed of sound ($M_G = 1.0$) and, second, 1/10 the speed of sound ($M_G = 0.1$). These results show that the pressure of the purged gas must be higher than 2×10^{-6} torr and the flow velocity of the purged gas near $M_G = 1$. Note that the mass ratio of the gas and the contaminant also influences the flux attenuation rate. A lower pressure gas may be sufficient to obtain a comparable result, if gas heavier than helium is used as a purged gas.

4.3.2 *Expansion of purged gas into vacuum*—The purged gas is eventually exhausted from the telescope through the sunshade into vacuum. An approximation for this expansion in the region far from the source, as shown in figure 14(a), is given by

$$U_G(r, \phi) = a_0 \sqrt{2/(\gamma - 1)} \quad (50)$$

$$n_G(r, \phi) = n_0(\phi)/r^2 \quad (51)$$

where a_0 is the speed of sound at the stagnation condition. This solution has two difficulties: (1) the solution becomes invalid in the source region (see fig. 14(b) and (2) the function $n_0(\phi)$ cannot be obtained from the conservation equations, although the solution is mathematically very simple. To circumvent these difficulties, the following methods are used. The function $n_0(\phi)$ is defined in the same form as in reference 35 as

$$n_0(\phi) = \alpha \cos^2(\pi\phi/2\phi) \quad (52)$$

where two constants α and ϕ are given for particular mass and momentum fluxes by the use of conservation relations. The source may be in the

telescope tube or the sunshade (as shown in fig. 14(b)) so that the flow field may be regarded as a point-source expansion. The position x_0 is determined by the use of a matching condition at the exit of the sunshade. This solution presents a flow field where the gas expands from a source only in the region limited by the limiting angle, ϕ , with a constant velocity U_G , and where the density decreases as $1/r^2$.

The values of α and ϕ are computed for the SIRTIF as

$$\alpha = 9.11 \times 10^{20} \times P_G (\text{torr})$$

$$\phi = 0.78\pi$$

The mass-flux rate at the exit of the sunshade is approximately written as

$$\dot{m}_G = A_{EX} \frac{\alpha}{x_0^2} a_0 \sqrt{\frac{2}{\gamma - 1}} \quad (53)$$

where A_{EX} is the cross-sectional area of the exit and the number density is assumed uniform; $x_0 = 163$ cm.

4.3.3 Interaction of purged gas with gaseous contaminant in space -

The purged-gas molecules will collide at most once with the contaminant molecules after they leave the tube and before they escape from the contaminant cloud. A rough estimate can be made by computing a quantity

$$x_{eff} = \int_{x_0}^{x_1} \frac{dx}{\lambda_{CG}(x)} \quad (54)$$

The result of this integration becomes

$$x_{eff} = \sigma_{CG} \alpha \left(0.976 + \frac{U_G}{U_c} \times 0.967 \right) \frac{1}{x_0} \quad (55)$$

Therefore, the attenuation of the oncoming contaminant could be estimated as

$$\frac{N_{11}}{N_{10}} = \exp(-x_{eff}) \quad (56)$$

where N_{10} is the oncoming flux for no purged gas and N_{11} is that attenuated by collisions with purged gas. The results are presented in figure 15 as a function of the pressure of the purged gas at the aperture and mass ratio, R_M , which is defined as the ratio of m_c to m_a . This indicates that the purged-gas pressure at the exit must be greater than 5×10^{-6} torr to be effective.

The total effect of the purged gas on the contaminant flux rate on the first mirror and the tube wall at the bottom is given by multiplying the effect in the tube by that in space (illustrated in fig. 16). Figure 16 shows that the flux rates will be 0.15% of N_{10} on the tube wall at the bottom for $P_G = 2 \times 10^{-6}$ torr, and $M_G = 1.0$ and $m_c/m_G = 5$.

4.3.4 *Interaction of particulate contaminant with purge gas*—Particulate contaminants are ejected from the Shuttle and are subjected to drag during collisions with ambient gas molecules. They may also interact with the purge gas near the telescope and some of them may cross through the FOV of the telescope. If their resident time in the FOV were considerably increased because of interactions with the purge gas, the purge-gas method of contamination control would be self-defeating (this effect is examined below).

The trajectories of particles moving under the influence of both ambient and purge-gas molecules are calculated to predict the resident times within the FOV. The computation is conducted for several sets of parameters such as the angle between the telescope axis and the satellite velocity vector, the purge-gas pressure, the particle diameter, the particle density, and several initial particle conditions.

A contaminant particle is assumed to be a sphere with a diameter D . The gas flow field consists of both purge gas and ambient gas molecules in free molecular flow. Both gases may be treated independently and the distribution functions of both gases are assumed to be Maxwellian. The number density of purge gas, n_G , is again defined as

$$n_G(r, \phi) = \alpha \cos^2(\pi\phi/2\phi)/r^2 \quad (57)$$

where r and ϕ are defined in figure 17 and α and ϕ are constants that depend on the purge-gas pressure. The values α and ϕ are computed for a pressure of 5.0×10^{-6} torr.

The velocity of a particle relative to the satellite may be neglected. Under such a flow condition, the drag caused by each gas flow is given by (ref. 36)

$$F_1 = \frac{\pi D^2 \rho_1 U_1^2}{8} \left\{ \frac{2 - \alpha_n + \alpha_t}{2S_1^3} \left[\frac{4S_1^4 + 4S_1^2 - 1}{2S_1} \operatorname{erf}(S_1) + \frac{2S_1^2 + 1}{\sqrt{\pi}} e^{-S_1^2} \right] + \frac{2\alpha_n}{3S_1} \sqrt{\frac{\pi T_c}{T_1}} \right\} \quad (58)$$

Here, subscript 1 indicates purge gas (G) or the ambient gas (a), respectively; ρ , α_n , α_t , and T_c are the density of gas, the normal and tangential momentum accommodation coefficients, and the temperature of the contaminant particle, respectively. A parameter S_1 is the speed ratio defined by

$$S_1 = U_1 \sqrt{h_1} = U_1 \sqrt{\frac{m_1}{2kT_1}}$$

An example from figure 17 is considered. The governing equations for the motion of a particle are given as

$$m_c \frac{d^2 r}{dt^2} - m_c r \left(\frac{d\phi}{dt} \right)^2 = F_{GO} \frac{a \cos^2(\pi\phi/2\phi)}{r^2} + F_a \cos(\phi + \theta) \quad (59)$$

$$\frac{d}{dt} \left(m_c r^2 \frac{d\phi}{dt} \right) = -r F_a \sin(\phi + \theta) \quad (60)$$

$$F_{GO} = \frac{\pi D^2 m_G U_G^2}{8} \left\{ \frac{2 - a_n + a_r}{2S_G^3} \left[\frac{4S_G^4 + 4S_G^2 - 1}{2S_G} \operatorname{erf}(S_G) + \frac{2S_G^2 + 1}{\sqrt{\pi}} e^{-S_G^2} \right] + \frac{2a_n}{3S_G} \sqrt{\frac{\pi T_G}{T_G}} \right\}$$

where θ is an angle between the vector \vec{U}_s and the axis (as defined in fig. 17) and m_c is the mass of a contaminant particle. These equations are numerically solved with various values of the particle ejection, velocity U_0 , angle δ , and location x (fig. 17). Analytical results are also used to reduce computational time for $F_G \ll F_a$. The boundary of the FOV is given as

$$\eta_F = \frac{100 - 0.0044(R - 500)}{2R} \quad (61)$$

The resident time within the FOV is given by the duration when

$$|\eta| \leq \eta_F \quad (62)$$

Values used in the computation are

$$\left. \begin{array}{l} U_s = 7.7 \text{ km/s} \\ m_a = 20 \text{ g/mole} \\ T_a = 1490 \text{ K} \\ \rho_a = 1.0 \times 10^{-14} \text{ g/cm}^3 \\ T_c = 300 \text{ K: assumed} \\ \text{Purge gas: helium} \end{array} \right\} \quad (Z = 400 \text{ km, ref. 37})$$

$$\rho_c = 1.0 \text{ g/cm}^3$$

$$T_G = 20 \text{ K}$$

$$P_G = 5.0 \times 10^{-6} \text{ torr}$$

$$\alpha = 9.11 \times 10^{20} \times P_G (\text{torr}) \left. \begin{array}{l} \phi = 0.7801 \pi \end{array} \right\} \text{ (given in sec. 4.3.2)}$$

Figure 18(a) and (b) illustrate particle trajectories with and without the purge gas. The resident times for several cases are presented in table 11. A general discussion concerning the effects of particle mass and initial ejection condition on their trajectories without the purge gas is presented in reference 38. In the present report, the influence of purge gas on the particle trajectory is discussed. Generally, the effect of purge gas is strongest near the telescope axis where the resident times of the particles within the FOV increase slightly. This influence sometimes decreases the resident time for the situation shown in figure 18(b). The influence of purge gas illustrated in figure 18(b) is larger because the particle trajectories almost coincide with the streamlines of the purge gas. The general feature of the particle effects does not qualitatively change with telescope angle θ if it is approximately $\pi/2$. The total number of contaminant particles that cross the FOV given condition could not be changed significantly by the influence of the purge gas.

CONCLUSIONS

The state of contaminant molecules, the deposition rate on surfaces of a cooled IR telescope, and the heat-transfer rate are estimated by the use of a zeroth-order approximation. It will take nearly 1 week for the cryodeposit to reach the critical thickness (tentative value $0.2 \mu\text{m}$) for a moderate oncoming contaminant flux rate without the purge gas. The critical thickness will be attained in a few days in the worst case. The magnitudes of the heat-flux rates transported from contaminant and purged gas were found to be comparable to the emissive power of a blackbody at 20 K.

It is natural that the attenuation rate of the contaminant flux strongly increases with an increase in the velocity of the purge gas for a given pressure. But it is less sensitive to the change in velocity if the mass-flow rate, which is proportional to the product of the pressure and the flow velocity, is kept constant. Such rarefied gas flow can be obtained by use of a number of diverging nozzles at the bottom of the telescope tube. For this technique to be sufficiently effective, the pressure of the purged gas must be more than 2×10^{-6} torr. The thickness of the cryodeposit will be $0.05 \mu\text{m}$ for $M_G = 0.1$ and $0.2 \mu\text{m}$ for $M_G = 0.1$ at the primary mirror for a 30-day mission for $P_G = 3 \times 10^{-6}$ torr; it will be thicker by more than one order of magnitude than the above thicknesses near the entrance aperture of the telescope under the same conditions.

The effect of purge-gas flow on particles was investigated. It was found that the only effect of the purge gas on the particulate contaminants was to slightly increase their resident times within the telescope FOV for a very small class of particles with unique particle ejection velocities and ejection angles.

Ames Research Center

National Aeronautics and Space Administration

Moffett Field, Calif., 94035, October 7, 1977

APPENDIX A

TELESCOPE GEOMETRIC VIEW FACTORS

The view factor F_{i-j} is defined as

$$F_{i-j} = \frac{1}{A_i} \int_{A_i} \int_{A_j} \frac{\cos \beta_i \cos \beta_j}{\pi r_{ij}^2} dA_i dA_j \quad (A1)$$

where r_{ij} is the distance between two area elements, dA_i and dA_j , β_i and β_j are the angles between r_{ij} and the normals to the surfaces, and the double integration is made over both areas A_i and A_j . For the geometry presented in figure 4, F_{2-1} and $F_{\delta 3-1}$ are expressed as

$$F_{2-1} = \frac{a_3^2}{a_3^2 - a_4^2} \left\{ \sqrt{\left(1 + \frac{a_4^2 + L^2}{a_3^2}\right)^2 - 4\left(\frac{a_4}{a_3}\right)^2} - \frac{L}{2a_3} \left[\sqrt{4 + \left(\frac{L}{a_3}\right)^2} + \sqrt{4\left(\frac{a_4}{a_3}\right)^2 + \left(\frac{L}{a_3}\right)^2} \right] \right\} \quad (A2)$$

$$\begin{aligned} F_{\delta 3-1} = & \frac{1}{2} - \frac{1}{2} \left[1 - \frac{a_4}{a_3} + \frac{x}{2a_3} - \frac{x^2 + 2a_3^2}{2a_3 \sqrt{4a_3^2 + x^2}} \right. \\ & + \frac{2a_4}{\pi a_3} \tan^{-1} \left(\frac{2\sqrt{a_3^2 - a_4^2}}{x} \right) + \frac{x}{\pi a_3} \sin^{-1} \left(1 - \frac{2a_4^2}{a_3^2} \right) \\ & - \frac{x^2 + 2a_3^2}{\pi a_3 \sqrt{4a_3^2 + x^2}} \sin^{-1} \frac{4(a_3^2 - a_4^2) + x^2(a_3^2 - 2a_4^2)/a_3^2}{x^2 + 4(a_3^2 - a_4^2)} \\ & + \frac{a_4}{a_3} - \frac{a_4}{\pi a_3} \cos^{-1} \frac{x^2 - a_3^2 + a_4^2}{x^2 + a_3^2 - a_4^2} \\ & + \frac{x}{\pi a_3} \frac{x^2 + a_3^2 + a_4^2}{\sqrt{(x^2 + a_3^2 + a_4^2) - 4a_3^2 a_4^2}} \cos^{-1} \frac{a_4(x^2 - a_3^2 + a_4^2)}{a_3(x^2 + a_3^2 - a_4^2)} \\ & \left. - \frac{x}{\pi a_3} \cos^{-1} \frac{a_4}{a_3} \right] \quad (A3) \end{aligned}$$

TABLE 1.- PROPERTIES OF AMBIENT MOLECULES

Parameters	Altitude, km			
	300	350	400	450
N_a (1/cm ² -sec)	7.6×10^{14}	3.3×10^{14}	1.6×10^{14}	8.0×10^{13}
T_a (K)	1432	1463	1487	1489
P_a (torr)	1.413×10^{-7}	6.294×10^{-8}	3.023×10^{-8}	2.053×10^{-8}
n_a (1/cm ³)	9.528×10^8	4.153×10^8	1.963×10^8	9.991×10^7
V_a (cm/sec)	1.157×10^5	1.208×10^5	1.256×10^5	1.294×10^5
M_a (g/mole)	22.66	21.24	19.94	18.82

$$N_a = n_a V_a \cos \theta: \quad \theta = 0, \quad V_s = 8 \text{ km/sec}$$

TABLE 2.- RETURN CONTAMINANT FLUX

Angle from z-axis, deg	Condition			
	Maximum return flux (with VERN and EVP), g/cm ² -sec		Minimum return flux (no VERN and EVP), g/cm ² -sec	
	Altitude, km			
	200	435	200	435
0	1.4×10^{-8}	2.8×10^{-10}	1.1×10^{-9}	4.4×10^{-11}
50 ± Y	3.0×10^{-8}	5.8×10^{-10}	1.1×10^{-9}	3.6×10^{-11}
25 ± Y	3.1×10^{-8}	6.0×10^{-10}	1.2×10^{-9}	4.3×10^{-11}
50 ± Y	3.0×10^{-8}	6.0×10^{-10}	1.1×10^{-9}	4.7×10^{-11}
45 - X	3.0×10^{-8}	6.0×10^{-10}	1.1×10^{-9}	4.7×10^{-11}
50 + X	2.9×10^{-9}	7.6×10^{-11}	1.6×10^{-9}	5.2×10^{-11}
50 - X	8.8×10^{-9}	2.1×10^{-10}	1.2×10^{-9}	6.2×10^{-11}

TABLE 3.- TIME REQUIRED FOR MONOLAYER TO FORM

N_1	View factor F			
	1.0	0.5	0.1	0.05
	Time, t_0			
$10^{12}/\text{cm}^2\text{-sec}$	13 min	25 min	2 hr, 10 min	4 hr, 10 min
$10^{15}/\text{cm}^2\text{-sec}$	0.8 sec	1.5 sec	8 sec	15 sec

TABLE 4.- VAPOR PRESSURE OF POSSIBLE CONTAMINANT

T, K	Vapor pressure of contaminant, torr					
	CO_2^a	CO^a	N_2^b	O_2^c	H_2^d	H_2O^e
15		1.7×10^{-21}	4.1×10^{-18}		100	
19		2.3×10^{-15}	1.0×10^{-12}		509	
20		3.4×10^{-14}	1.0×10^{-11}	1.0×10^{-15}	700	
21		3.7×10^{-13}	9.0×10^{-11}	1.6×10^{-13} (22 K)	935	
30		7.9×10^{-17}	3.0×10^{-5}	α -solid (23.78 K) 1.2×10^{-7}		
40	7.2×10^{-26}	4.0×10^{-3}	4.3×10^{-2}	1.2×10^{-3} β -solid (43.77 K)		
50	9.0×10^{-19}	6.6×10 α -solid (61.5 K)	3.0 solid (63.15 K)	2.2×10^{-1} γ -solid (54.35 K)		
77	8.5×10^{-9}	β -solid (68.1 K) 432 (liquid)	1335 (liquid)	1.3×10^2 (75 K, liquid)		1.5×10^{-5} (175 K)

^aReference 16^bReference 17^cReference 18^dReference 19^eReference 20

TABLE 5.- HEAT OF SUBLIMATION

Temperature, K	Molecules, kcal/mole					
	CO ₂ ^a	CO ^a	N ₂ ^b	O ₂ ^c	H ₂ ^d	H ₂ O ^e
15		2.0	1.7		0.22	
19		2.0	1.8		.22	
20		2.0	1.8	2.2	.22	
21		2.0	1.8	2.2 (22 K) α-solid (23.78 K)	.21	
30		2.0	1.8	2.2		
40	6.5	2.0	1.7	2.2 β-solid (43.77 K)		
50	6.5	2.0 α-solid (61.5 K)	1.7	2.0		
			solid	γ-solid (54.35 K)		
77	6.5	β-solid (68.1 K) 1.5 (liquid)	1.3 (liquid)	1.7 (76 K liquid)		12 (-173 K)

^aReference 16^bReference 17^cReference 18^dReference 19^eReference 21

TABLE 6.- STICKING COEFFICIENT OF CO₂ ON CO₂ DEPOSITED LAYER
(T_w is surface temperature, and T_G is gas temperature)

T _w , K	Sticking coefficient, α _s T _G , K					
	195	202	205	209	300	150- 400
10	1.0 ^a				0.75 ^a	
12.5	.98 ^a				.70 ^a	
15	.96 ^a				.67 ^b	0.50
17.5	.92 ^a				.65 ^b	.49
20	.90 ^a				.63 ^b	.49
21			1.00 ± 0.01 ^a			
22.5	.87 ^a				.63	.49
25	.85 ^a				.63	.49
55				0.99 ^b		
74					1.0 ^b	
77	.85 ^a				.63 ^b .95 ^b .85 ^b .99 ^c	.49
79						1.0 ^d
80.5		0.86 ^a				

^aReference 22

^bReference 23

^cReference 24

^dPaper by B. A. Buffman, P. B. Henault, and R. A. Flinn, Vac. Symp. Trans., Vol. 9, 1962, p. 216.

TABLE 7.- STICKING COEFFICIENTS OF CONTAMINANT MOLECULES ^a

T_w , K	T_G , K		
	77	300	400
CO on CO deposited layer			
10	1.0	0.90	0.73
12.5	↓	.85	↓
15		↓	
↓		↓	
25		↓	
N ₂ on N ₂ deposited layer			
10	1.0	0.65	0.49
12.5	.99	.63	↓
15	.96	.62	
17.5	.90	.61	
20	.84	.60	
22.5	.80	.60	
25	.79	.60	
O ₂ on O ₂ deposited layer			
20	1.0	0.86	---

^aReference 25

TABLE 8.- STICKING COEFFICIENT OF He

T_w , K	T_G , K	α_s	Surface condition	Reference
4.2	4.2	0.9	* Molecular sieve 5Å	26
4 - 5.2	290	.480	Ar precondensed layer, low coverage	27
↓	↓	.480	Ar precondensed layer, high coverage	↓
		.380	Kr precondensed layer, low coverage	
		.410	Kr precondensed layer, high coverage	
		.370	Xe precondensed layer, low coverage	
		.470	Xe precondensed layer, high coverage	↓
10	77	4.8×10^{-2}	* Molecular sieve 5Å	28
13.6	77	3.7×10^{-3}	* Molecular sieve 5Å	28
17	77	---	* Molecular sieve 5Å	28

TABLE 9.- ENERGY FLUX RATE DURING CO₂ DEPOSITION

Energy flux rates, cal/cm ² / sec	Return flux rate, molecules/cm ² /sec					
	10 ¹³		10 ¹²		10 ¹¹	
	Sticking coefficient, α _s					
	1.0	0.5	1.0	0.5	1.0	0.5
E _k	4.9×10 ⁻⁸	2.5×10 ⁻⁸	4.9×10 ⁻⁹	2.5×10 ⁻⁹	4.9×10 ⁻¹⁰	2.5×10 ⁻¹⁰
E _d	1.11×10 ⁻⁷	5.5×10 ⁻⁸	1.1×10 ⁻⁸	5.5×10 ⁻⁹	1.1×10 ⁻⁹	5.5×10 ⁻¹⁰
E _{ac}	0	2.0×10 ⁻⁸	0	2.0×10 ⁻⁹	0	2.0×10 ⁻¹⁰
E	1.6×10 ⁻⁷	1.0×10 ⁻⁷	1.6×10 ⁻⁸	1.0×10 ⁻⁸	1.6×10 ⁻⁹	1.0×10 ⁻⁹

TABLE 10.- ENERGY FLUX RATE



Molecules	Return flux rate, molecules/cm ² /sec			
	10 ¹³	10 ¹²	10 ¹¹	10 ¹⁰
CO	8.2×10 ⁻⁸	8.2×10 ⁻⁹	8.2×10 ⁻¹⁰	8.2×10 ⁻¹¹
N ₂	7.8×10 ⁻⁸	7.8×10 ⁻⁹	7.3×10 ⁻¹⁰	3.2×10 ⁻¹¹
O ₂	8.6×10 ⁻⁸	8.6×10 ⁻⁹	8.6×10 ⁻¹⁰	8.6×10 ⁻¹¹
H ₂ O	2.6×10 ⁻⁷	2.6×10 ⁻⁸	2.6×10 ⁻⁹	2.6×10 ⁻¹⁰
H ₂	~1×10 ⁻⁸	~1×10 ⁻⁹	~1×10 ⁻¹⁰	~1×10 ⁻¹¹

TABLE 11.- RESIDENT TIME OF PARTICLES IN FOV

U_0 , cm/sec				
δ , deg	50	80	80, $P_G = 0$	200
	Diam = 5μ , $\theta = 90^\circ$, $x = -1000$ cm			
45	N	N	N	0.44
60	N	0.55	0.50	.48
90	0.55	.50	.54	.56
120	.55	.50	.50	.50
150	N	.50	.48	.42
	Diam = 5μ , $\theta = 90^\circ$, $x = -300$ cm			
60	N	N	N	N
90	N	N	N	1.02
120	N	1.0	0.88	.74
	80	100	200	200, $P_G = 0$
	Diam = 5μ , $\theta = 90^\circ$, $x = 500$ cm			
120	N	N	N	N
135	↓	↓	3.08	5.58
140			5.78	N
150			N	N
	100		100, $P_G = 0$	
	Diam = 5μ , $\theta = 70^\circ$, $x = -1000$ cm			
60	0.60		0.55	
90	.60		.55	
120	.55		.55	
	20	50	80	200
	Diam = 100μ , $\theta = 90^\circ$, $x = -1000$ cm			
45	N	1.85	1.40	0.70
60	2.35	2.05	1.75	.96
90	2.40	2.50	2.65	3.20
120	2.35	2.80	2.20	2.45
150	---	2.15	1.55	1.50

Note: N denotes that the particle does not cross FOV.

TABLE 11.- Continued

U_o , cm/sec				
δ , deg	50	100	100, $P_G = 0$	200
	Diam = 100 μ , $\theta = 90^\circ$, $x = 1000$ cm			
95	N	N	N	N
100		N		7.56
105		N		2.58
110		8.0		1.72
120		2.65	4.35	1.06
130	20.8	1.85	2.20	.80
150	N	N	1.35	N

REFERENCES

1. Anon.: Final Report of the Space Shuttle Payload Planning Working Groups. Astronomy, vol. 1, NASA Goddard Space Flight Center, May 1976.
2. Kovach, W. S.: Astronomy Working Group's Recommended Contamination Limits for Astronomy Sortie Missions, Contract NAS 8-29462, GDCA-DDA-72-009, Oct. 1973.
3. Bareiss, L. E.; Rantanen, R. O.; and Ress, E. B.: Payload/Orbiter Contamination Control Requirement Study. Contract NAS 8-30452. NASA CR-120379, 1974.
4. Thomas, Lloyd B.: Thermal Accommodation of Gases on Solids, in Fundamentals of Gas-Surface Interactions (H. Saltsburg *et al.*, ed.), (1967) pp. 346.
5. Viehmann, Walter; and Eubanks, Alfred G.: Effects of Surface Contamination on the Infrared Emissivity and Visible-Light Scattering of Highly Reflective Surfaces at Cryogenic Temperature. NASA TN D-6585, Feb. 1972.
6. Wood, B. E.; Smith, A. M.; Roux, J. A.; and Seiber, B. A.: Spectral Absolute Reflectance of CO₂ Frosts from 0.5 to 12.0 μ . AIAA J., vol. 9, no. 7, July 1971, p. 1338-1344.
7. Wood, B. E.; Smith, A. M.; Roux, J. A.; and Seiber, B. A.: Spectral Infrared Reflectance of H₂O Condensed on LN₂-Cooled Surfaces in Vacuum. AIAA J., vol. 9, no. 9, Sept. 1971, pp. 1836-1842.
8. Seiber, B. A.; Smith, A. M.; Wood, B. E.; and Müller, P. R.: Refractive Indices and Densities of H₂O and CO₂ Films Condensed on Cryogenic Surfaces. Appl. Opt., vol. 10, no. 9, Sept. 1971, pp. 2086-2081.
9. Liu, C. K.; and Tien, C. L.: Cryocontamination of Optical Solar Reflectors and Mirrors. Adv. Cryogen. Eng., vol. 19, 1974, pp. 474-481.
10. Liu, C. K.: Degradation of Cold Optical Systems by Cryodeposition. LMSC/D266319, TP-3347, Lockheed-Palo Alto Res. Lab., Feb. 1972.
11. Thompson, S. B.; Arnold, F.; and Sanderson, R. B.: Optical Effects of Cryodeposits on Low Scatter Mirrors. AIAA Paper 73-732, July 1973.
12. Young, R. P.: Degradation of Low Scatter Mirrors by Particle Contamination. AIAA Paper 75-667, May 1975.
13. Tuzi, Y.; Kobayashi, M.; and Asao, K.: Adsorption of Mixed Gases on a Pyrex Glass Surface at Very Low Pressure. J. Vac. Sci. Tech., vol. 9, no. 1, Jan/Feb. 1972, pp. 248-252.

14. Hobson, J. P.: Physical Adsorption at Extremely Low Pressures, in The Solid-Gas Interface (E. A. Flood, ed.), vol. I, Ch. 14, Marcel Dekker, Inc., 1967.
15. de Boer, J. H.: The Dynamical Character of Adsorption. Oxford, Clarendon Press, 1953.
16. Mullins, J. C.; Kirk, B. S.; and Ziegler, W. T.: Calculation of the Vapor Pressure and Heats of Vaporization and Sublimation of Liquids and Solids, Especially Below One Atmosphere. V. Carbon Monoxide and Carbon Dioxide, Rep. NBS Contract CST-7404, Georgia Inst. of Tech., Boulder, Colorado, 1963.
17. Mullins, J. C.; and Ziegler, W. T.: Calculation of the Vapor Pressure and Heats of Vaporization and Sublimation of Liquids and Solids, Especially Below One Atmosphere. VI Nitrogen and Fluorine, Rep. no. 1, CST-7404, Georgia Inst. of Tech., 1963.
18. Mullins, J. C.; Ziegler, W. T.; and Kirk, B. S.: The Thermodynamic Properties of Oxygen from 20° to 100°K. Adv. in Cryogen. Eng., vol. 8, 1962, pp. 126-134.
19. Mullins, J. C.; Ziegler, W. T.; and Kirk, B. S.: The Thermodynamic Properties of Parahydrogen from 1° to 22°K. Adv. Cryogen. Eng., vol. 8, 1962, pp. 116-125.
20. Gray, D. E., ed.: American Institute of Physics Handbook, Section 4-274, New York McGraw Hill, 1963.
21. Davy, J. Gordon; and Somorjai, G. A.: Studies of the Vaporization Mechanism of Ice Single Crystals. J. Chem. Phys., vol. 55, no. 8, 1971, pp. 3624-3636.
22. Levenson, Leonard L.: Condensation Coefficient of Argon, Krypton, Xenon, and Carbon Dioxide Measured with a Quartz Crystal Microbalance. J. Vac. Sci. Tech., vol. 8, no. 5, Sept./Oct. 1971, pp. 629-635.
23. Brown, R. F.; Trayer, D. M.; and Busby, M. R.: Condensation of 300-2500 K Gases on Surfaces at Cryogenic Temperatures. J. Vac. Sci. Technol., vol. 7, Jan./Feb. 1970, pp. 241-246.
24. Moody, T. L.: Capture Coefficient of 300°K CO₂ on a 77°K Surface as Measured by the Rotating Gage Technique. AEDC-TR-66-231, Jan. 1967.
25. Dawson, J. P.; and Haygood, J. D.: Cryopumping. Cryogenics, vol. 5, no. 2, April 1965, pp. 57-67.
26. Grenier, G. E.; and Stern, S. A.: Cryosorption Pumping of Helium at 4.2°K. J. Vac. Sci. Tech., vol. 3, no. 6, Dec. 1966, pp. 334-337.

27. Lee, T. J.: The Physical Adsorption of Helium on Solid Argon, Krypton, and Xenon. *Surface Sci.*, vol. 44, no. 2, Aug. 1974, pp. 389-400.
28. Southerlan, R. E.: 10-22 K Cryosorption of Helium on Molecular Sieve 5A and Hydrogen on Condensed Vapors. *Tech. Doc. Rep. AEDC-TR-65-49*, May 1965.
29. Cercignani, C.; and Sernagiotto, F.: Cylindrical Poiseuille Flow of a Rarefied Gas. *Phys. Fluids*, vol. 9, no. 1, Jan. 1966, pp. 40-44.
30. Ferziger, J. H.: Flow of a Rarefied Gas through a Cylindrical Tube. *Phys. Fluids*, vol. 10, no. 7, July 1967, pp. 1448-1453.
31. Sone, Yoshio; and Yamamoto, Kyasi: Flow of Rarefied Gas through a Circular Pipe. *Phys. Fluids*, vol. 11, no. 8, Aug. 1968, pp. 1672-1678.
32. Sreekanth, A. K.: Some Experiments on the Flow of a Rarefied Gas through a Circular Orifice. *Proc. 4th Intern. Symp. on Rarefied Gas Dynamics*. Academic Press, 1965.
33. Sreekanth, A. K.: Transition Flow through Short Circular Tubes. *Phys. Fluids*, vol. 8, no. 11, Nov. 1965, pp. 1951-1956.
34. Milligan, Mancil W.: Low-Density Gas Flow in Long Tubes. *AIAA J.*, vol. 4, no. 4, Apr. 1966, pp. 745-746.
35. Grundy, R. E.: Axially Symmetric Expansion of a Monatomic Gas from an Orifice into a Vacuum. *Phys. Fluids*, vol. 12, no. 10, Oct. 1969, pp. 2011-2018.
36. Kogan, M. N.: *Rarefied Gas Dynamics*. New York Plenum Press, 1969.
37. Anon.: *U. S. Standard Atmosphere*, 1962.
38. Simpson, J. P.: and Witteborn, F. C.: Effect of the Shuttle Contaminant Environment on a Sensitive Infrared Telescope. *Applied Optics*, vol. 16, no. 8, Aug. 1977, pp. 2051-2073.

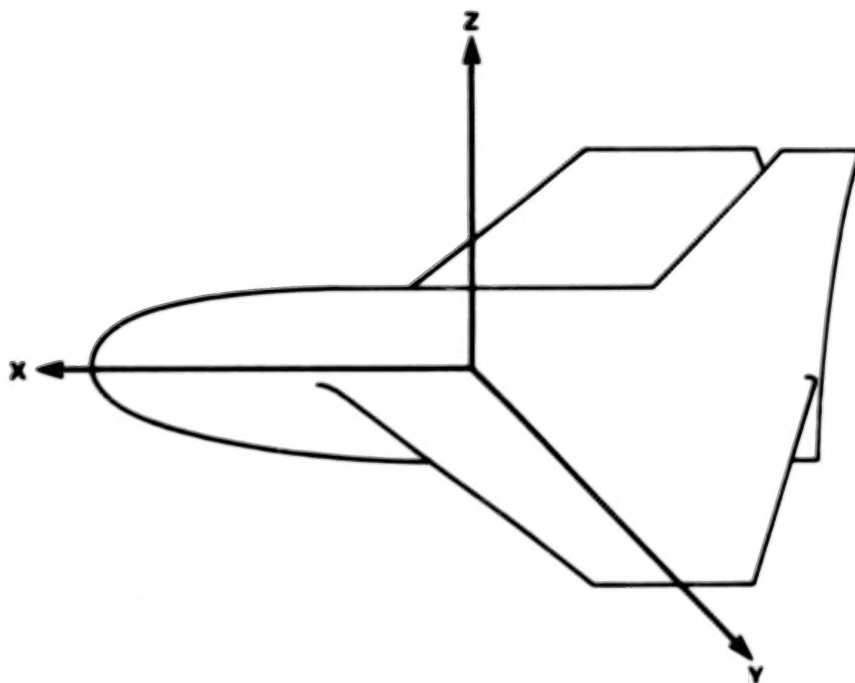


Figure 1.- Shuttle coordinate system.

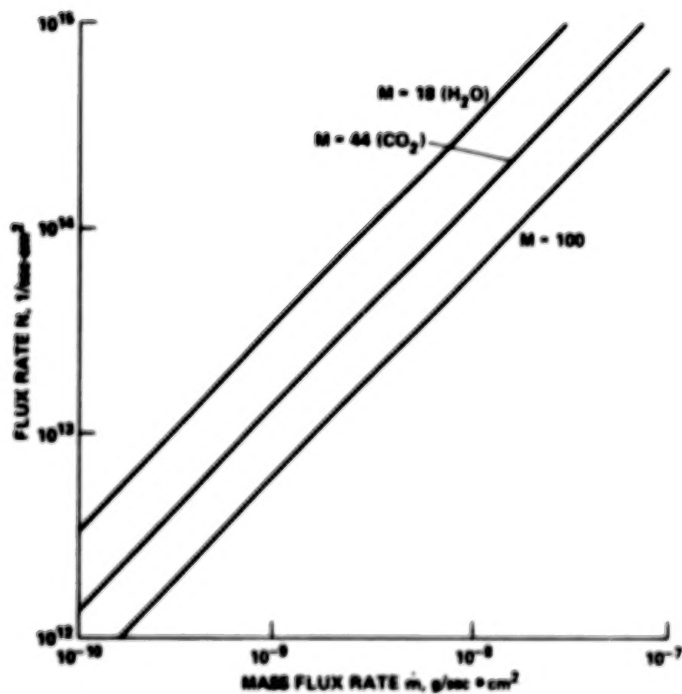


Figure 2.- Conversion data from the mass flux rate to the return flux rate N (1/cm²-sec).

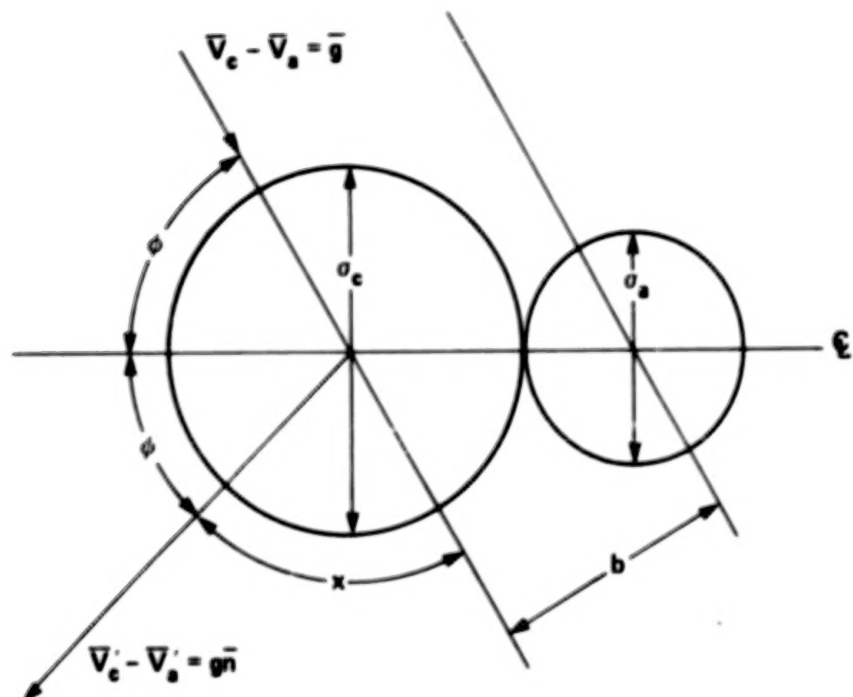


Figure 3.- Collision geometry.

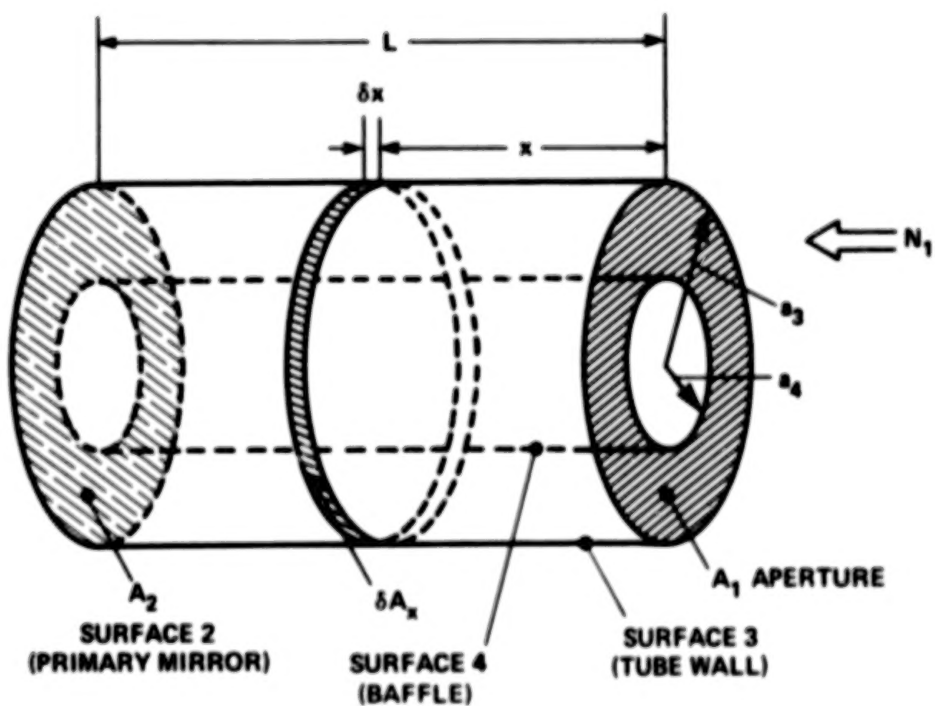


Figure 4.- Physical model of the SIRTf contamination problem.

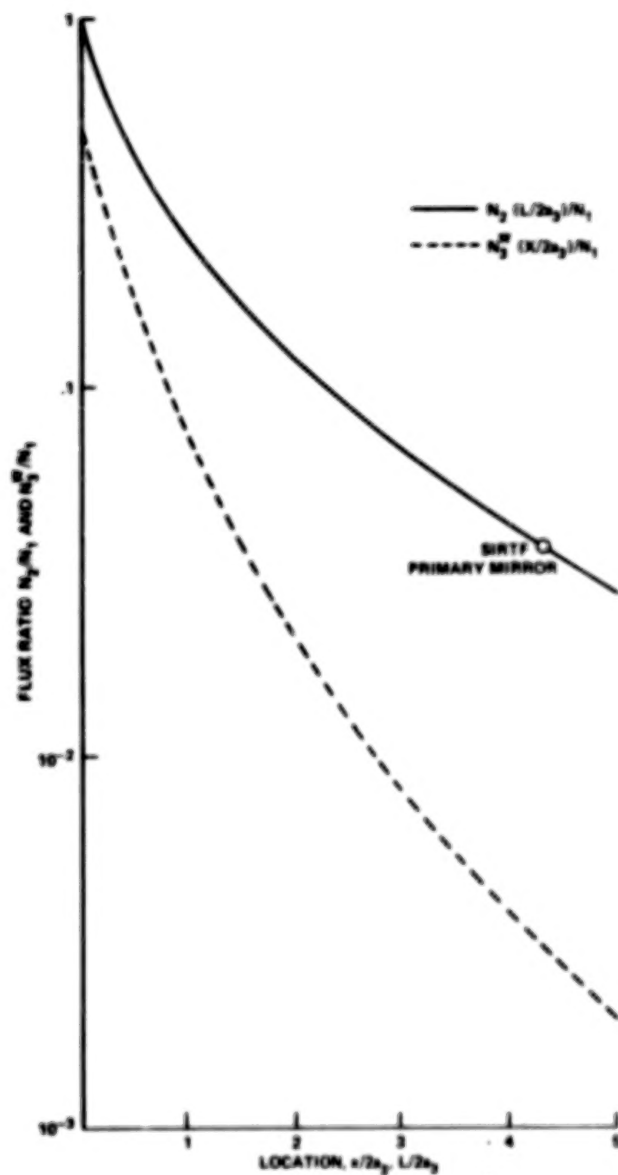


Figure 5.- Contaminant flux rate without purge gas.

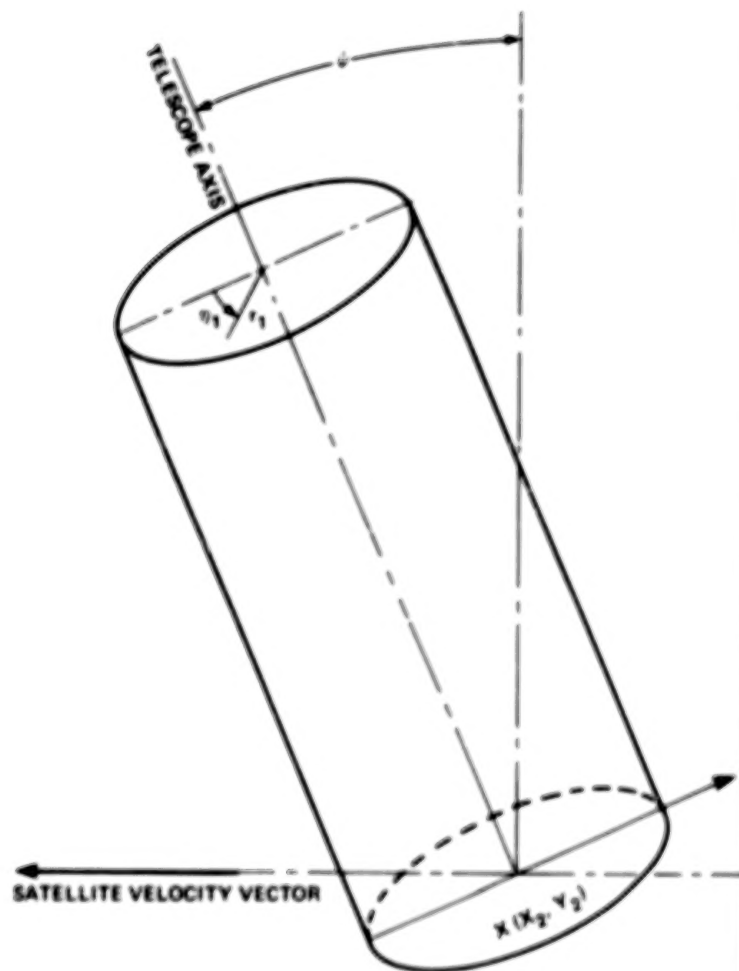
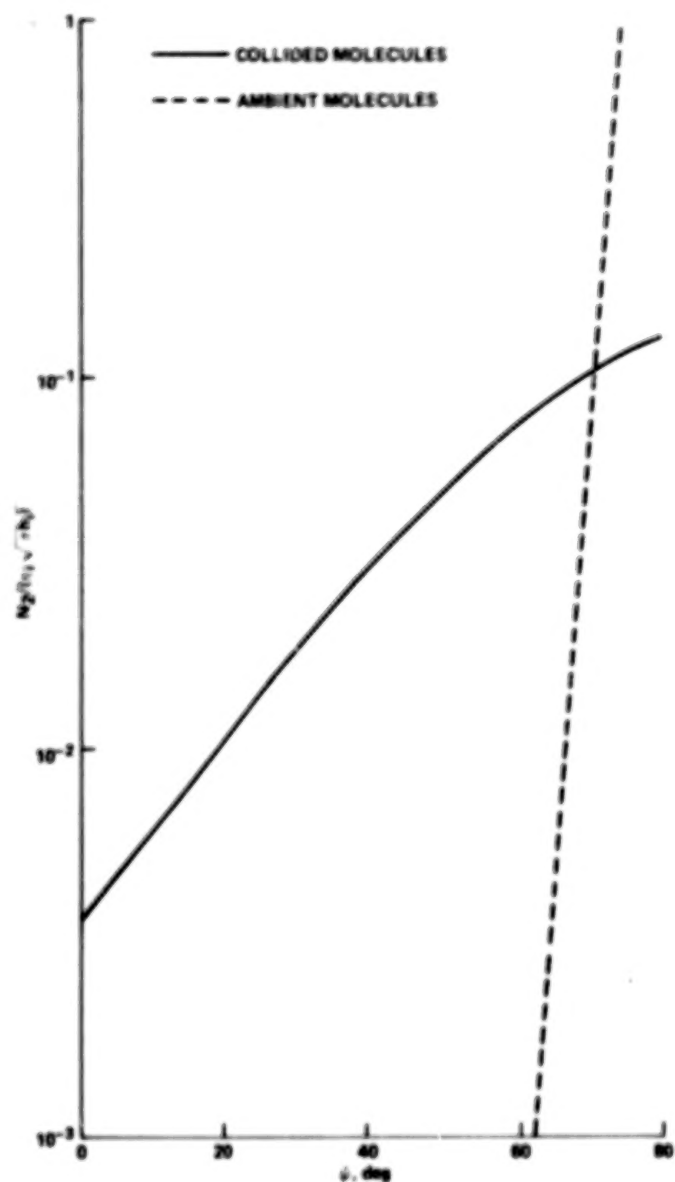
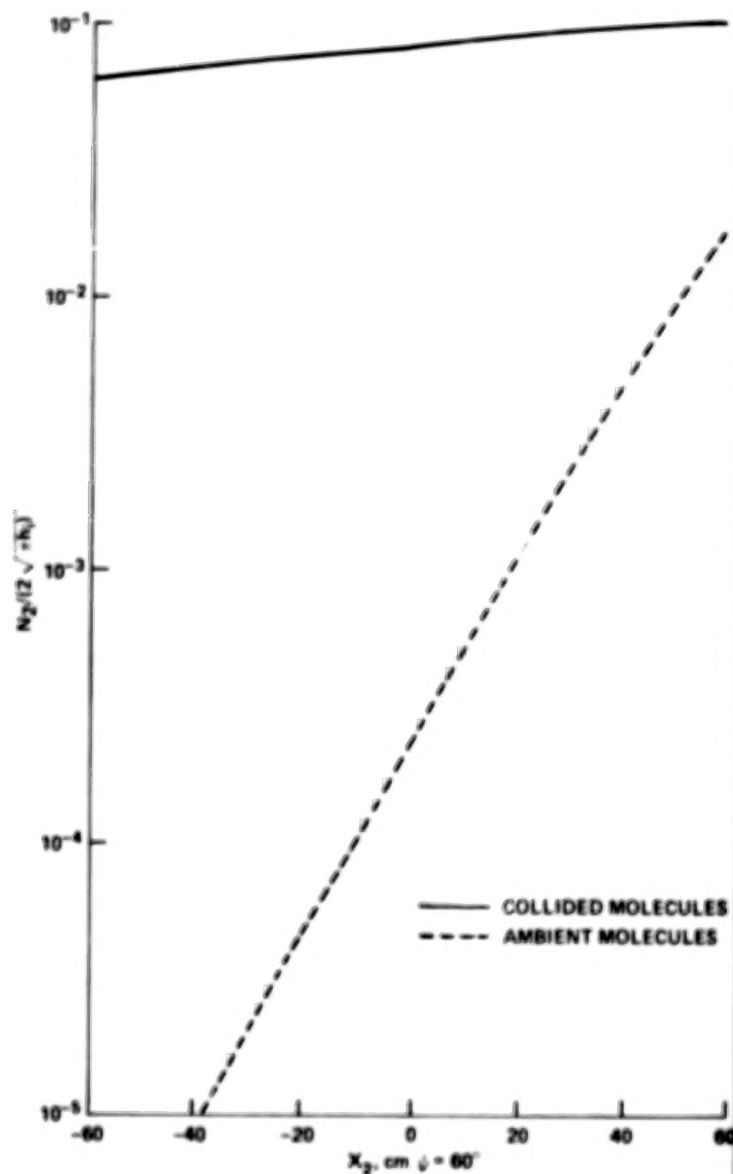


Figure 6.- Definition of telescope inclination

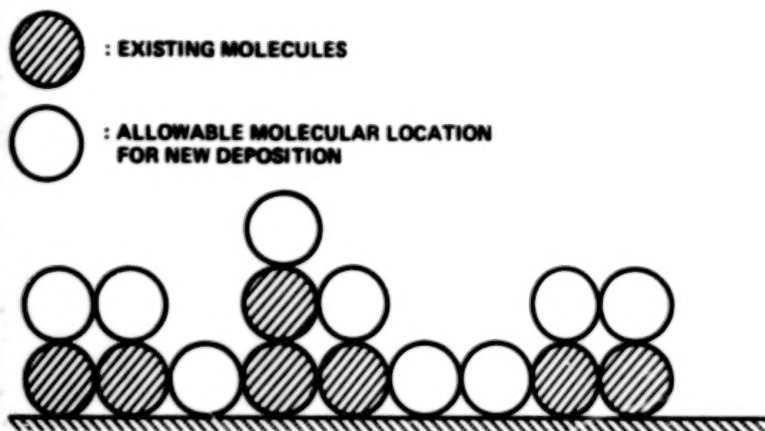


(a) Distribution on primary mirror vs telescope inclination.

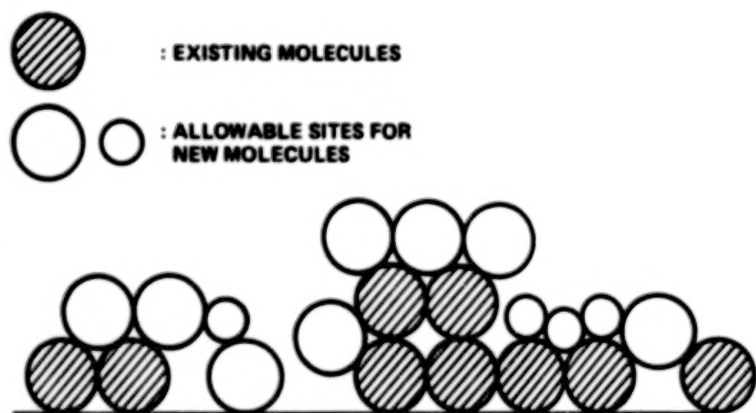


(b) Distribution on primary mirror.

Figure 7.- Nondimensionalized flux rate.



(a) Sites in BET assumption.



(b) With low surface diffusion.

Figure 8.- Allowable adsorption.

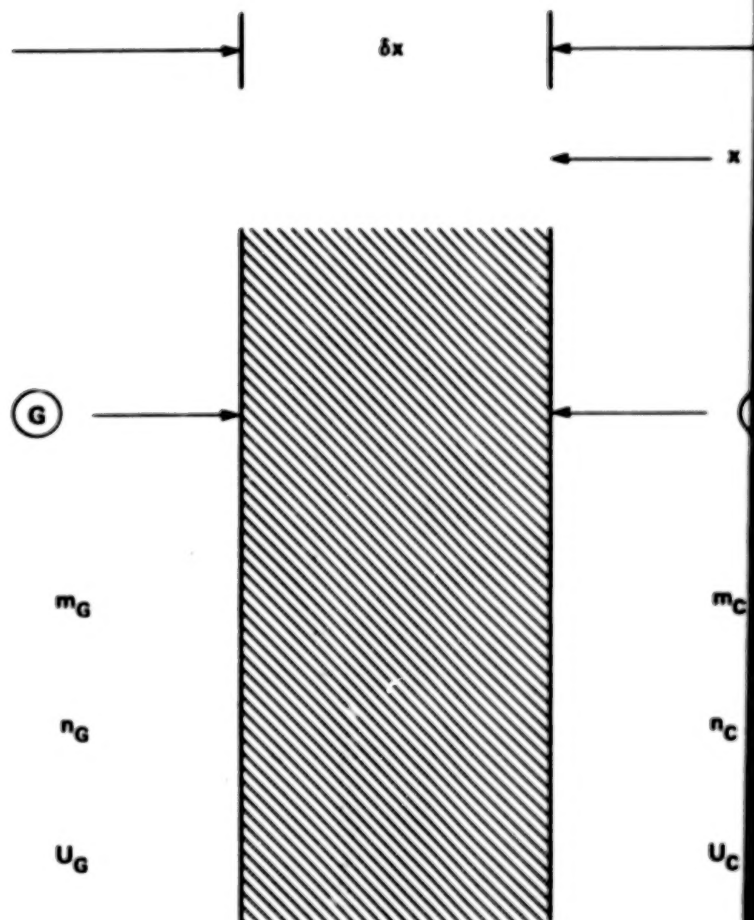


Figure 9.- Interaction of gaseous contaminant with purge gas.

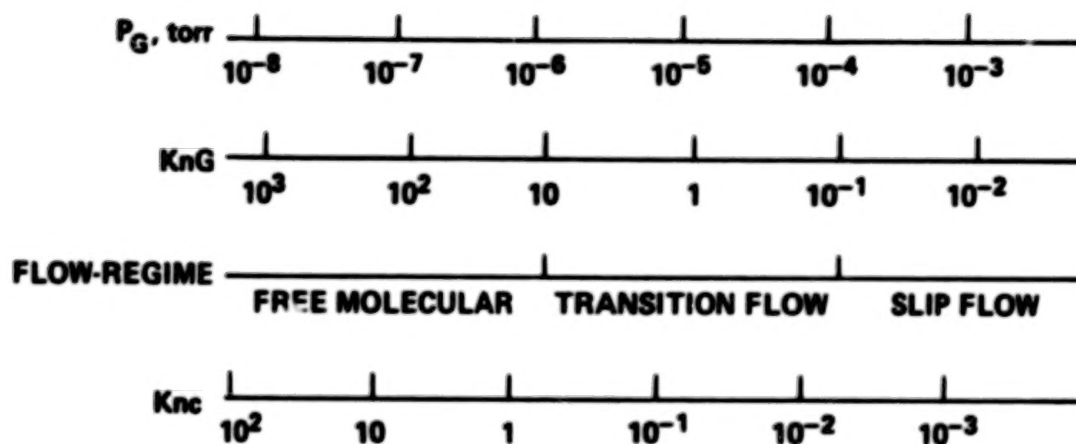


Figure 10.- Purge pressure and purged-gas flow.

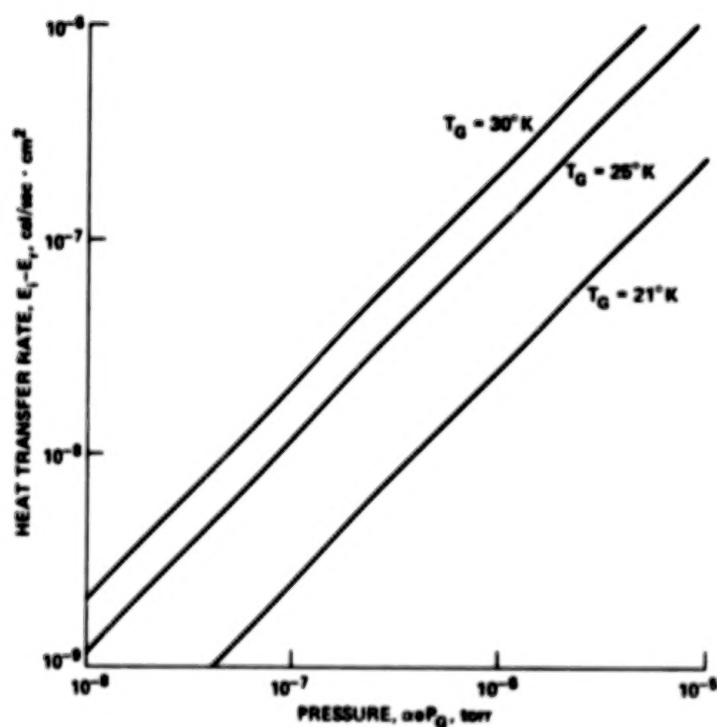


Figure 11.- Heat-transfer rate from the purged-gas flow to telescope tube.



Figure 12.- Physical model of attenuation of contaminant flux.

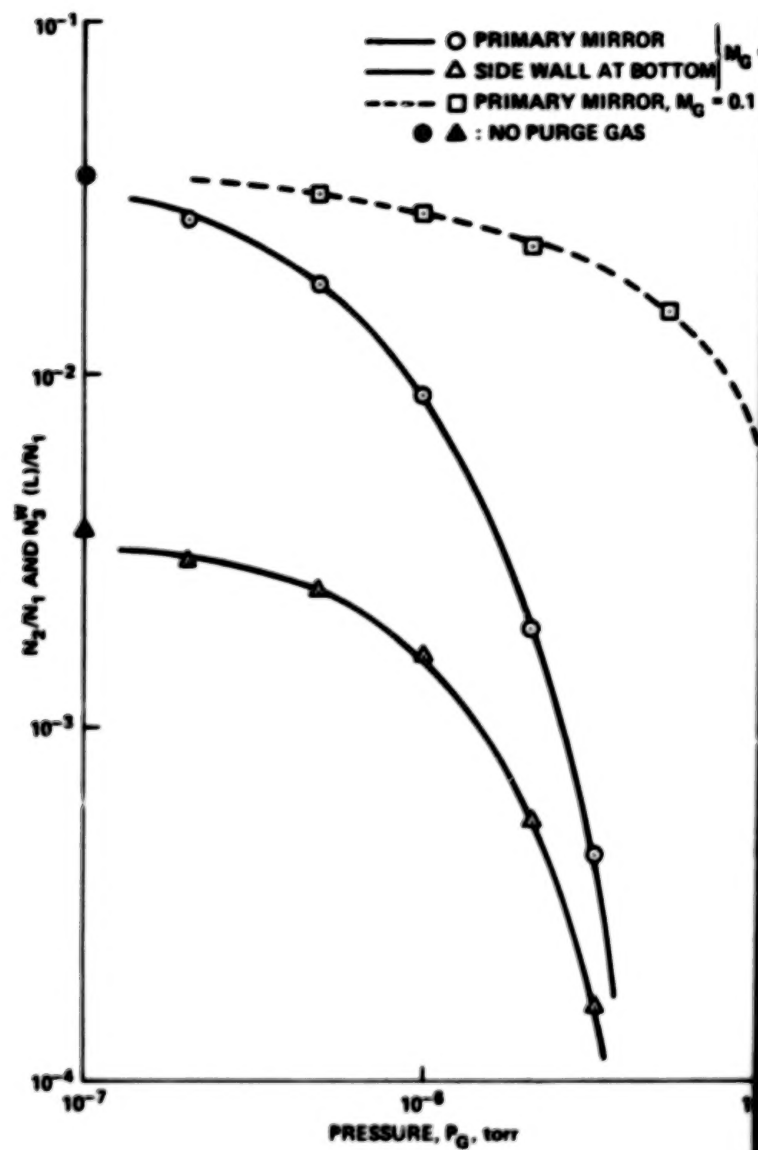


Figure 13.- Effect of purge gas.

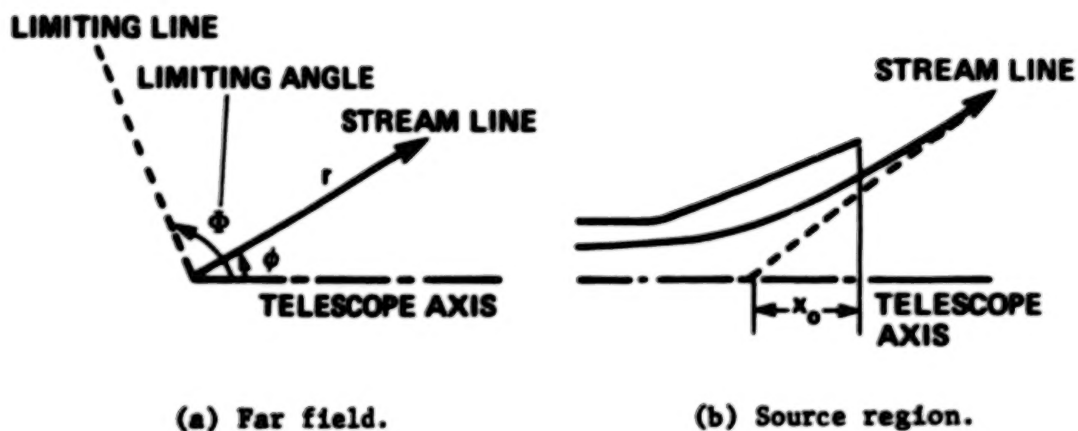


Figure 14.- Purged-gas flow field.

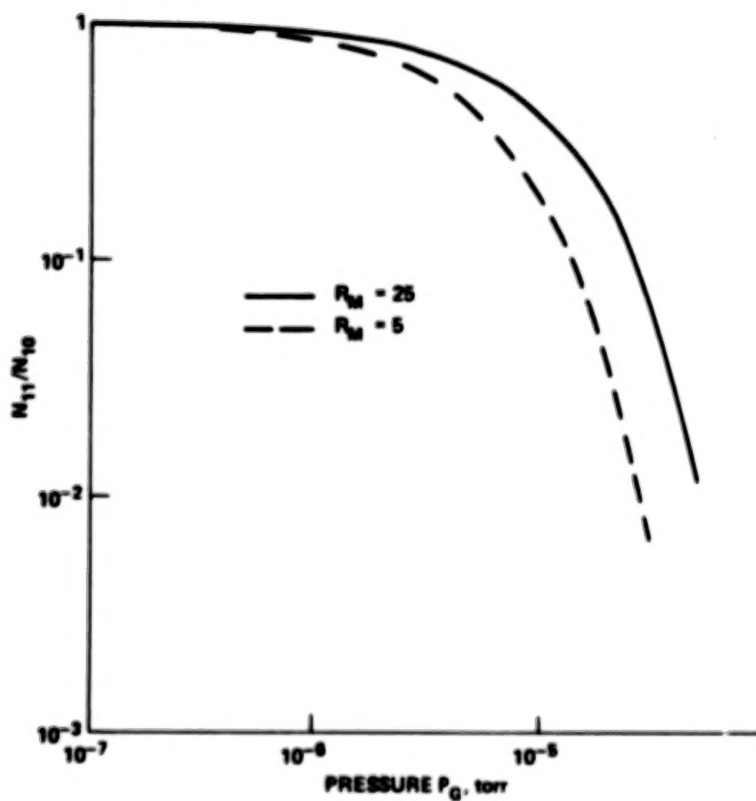
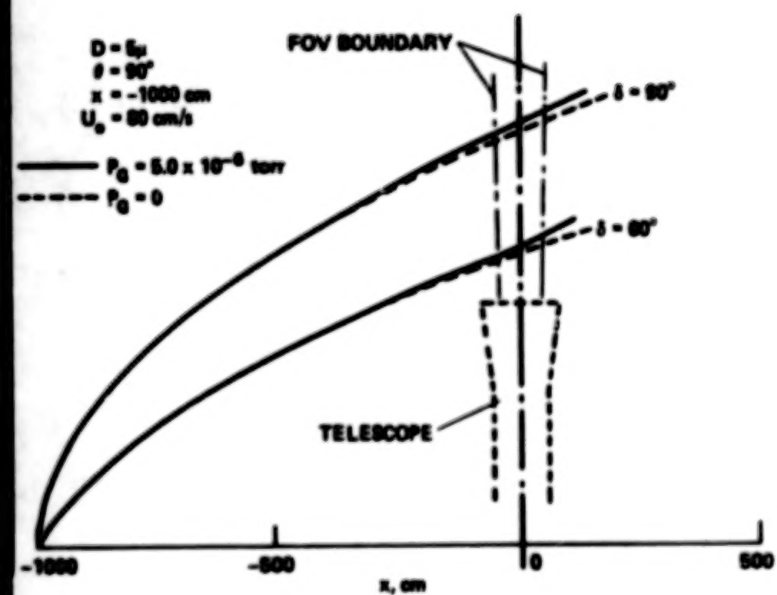
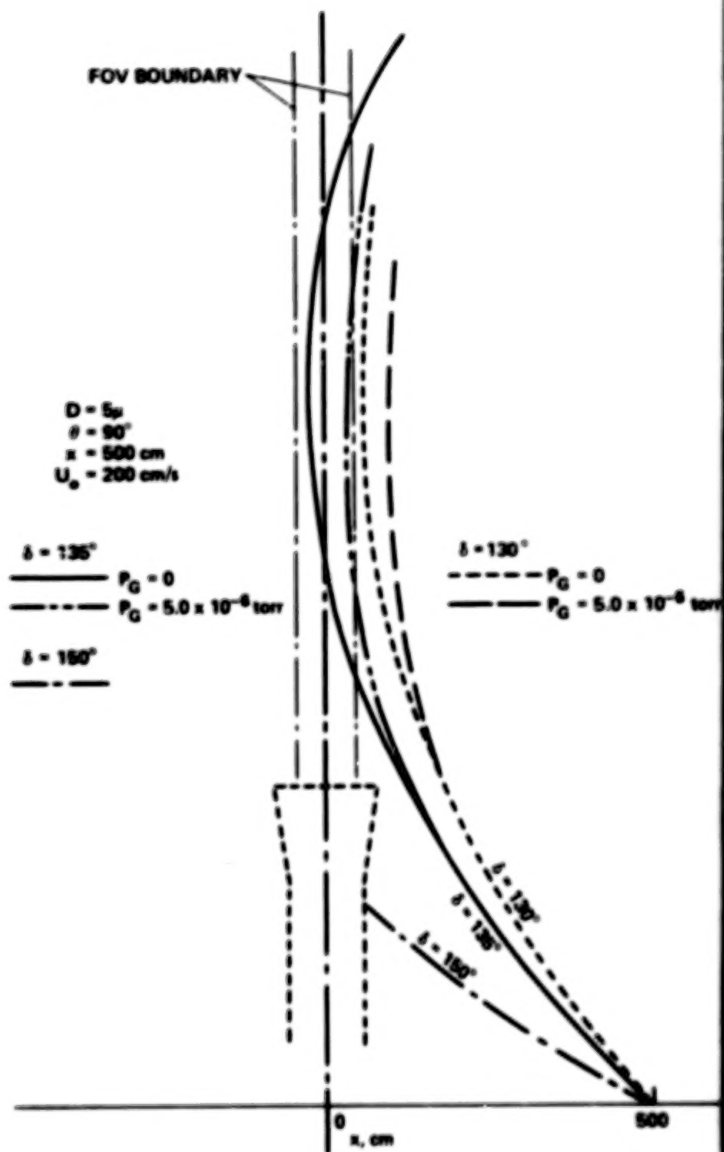


Figure 15.- Attenuation of oncoming contaminant flux in space.



(a) In front of the telescope.



(b) From back side of the telescope.

Figure 18.- Trajectories of particles ejected.

1 Report No NASA TP-1177		2 Government Accession No		3 Recipient's Catalog No	
4 Title and Subtitle THEORETICAL CONTAMINATION OF CRYOGENIC SATELLITE TELESOPES				5 Report Date April 1978	
				6 Performing Organization Code	
7 Author(s) M. Murakami*				8 Performing Organization Report No A-7024	
9 Performing Organization Name and Address NASA Ames Research Center Moffett Field, Calif. 94035				10 Work Unit No 506-25-21-02-00	
				11 Contract or Grant No.	
12 Sponsoring Agency Name and Address National Aeronautics and Space Administration Washington, D.C. 20546				13 Type of Report and Period Covered Technical Paper	
				14 Sponsoring Agency Code	
15 Supplementary Notes *National Research Council Research Associate; presently at the Institute of Space and Aeronautical Science, University of Tokyo, Tokyo, Japan					
16 Abstract Contamination problems which are caused by deposition of condensible gas molecules on cryogenically cooled satellite telescopes are theoretically investigated. The state of contaminant molecules, the deposition rate on key surfaces, and the heat-transfer rate are estimated by the use of a zeroth-order approximation. Optical surfaces of infrared telescopes cooled to about 20 K should be considered to be covered with at least several deposition layers of condensible molecules without any contamination con- trols. The effectiveness of the purge-gas method of contamination controls is discussed. This method attempts to drive condensible molecules from the telescope tube by impacts with a purge gas in the telescope tube. For this technique to be sufficiently effective, the pressure of the purge gas must be more than 2×10^{-6} torr. The influence caused by interactions of the purged gas with the particulate contaminants are found to slightly increase the resident times of the particulate contaminants within the telescope field of view.					
17 Key Words (Suggested by Author(s)) Spacecraft contamination Condensation and contamination control				18 Distribution Statement Unlimited STAR Category - 15	
19 Security Class. (of this report) Unclassified		20 Security Class. (of this page) Unclassified		21 No. of Pages 48	
				22 Price* \$4.00	

*For sale by the National Technical Information Service, Springfield, Virginia 22161

NASA-Langley, 1978